Hydrogen Material Compatibility

Steel Embrittlement

Dr Arief Dahoe

Explosion, Hydrogen Safety and Combustion Scientist



Dutch Armed Forces

Knowledge Center for Explosion and Hydrogen Safety

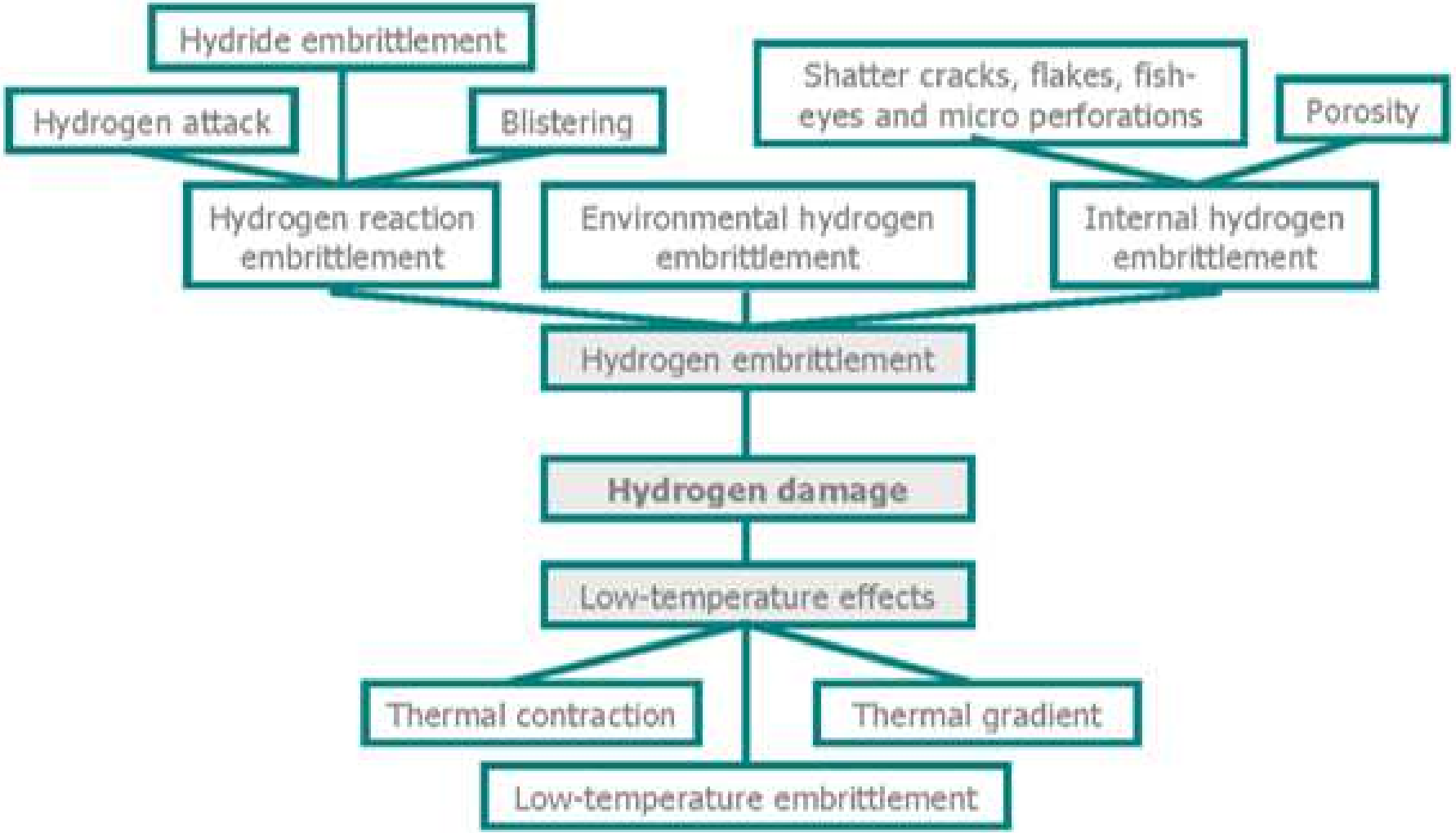
http://www.explosionsolutions.org/kcehs/

ACKNOWLEDGEMENTS

UNIVERSITY OF CAMBRIDGE

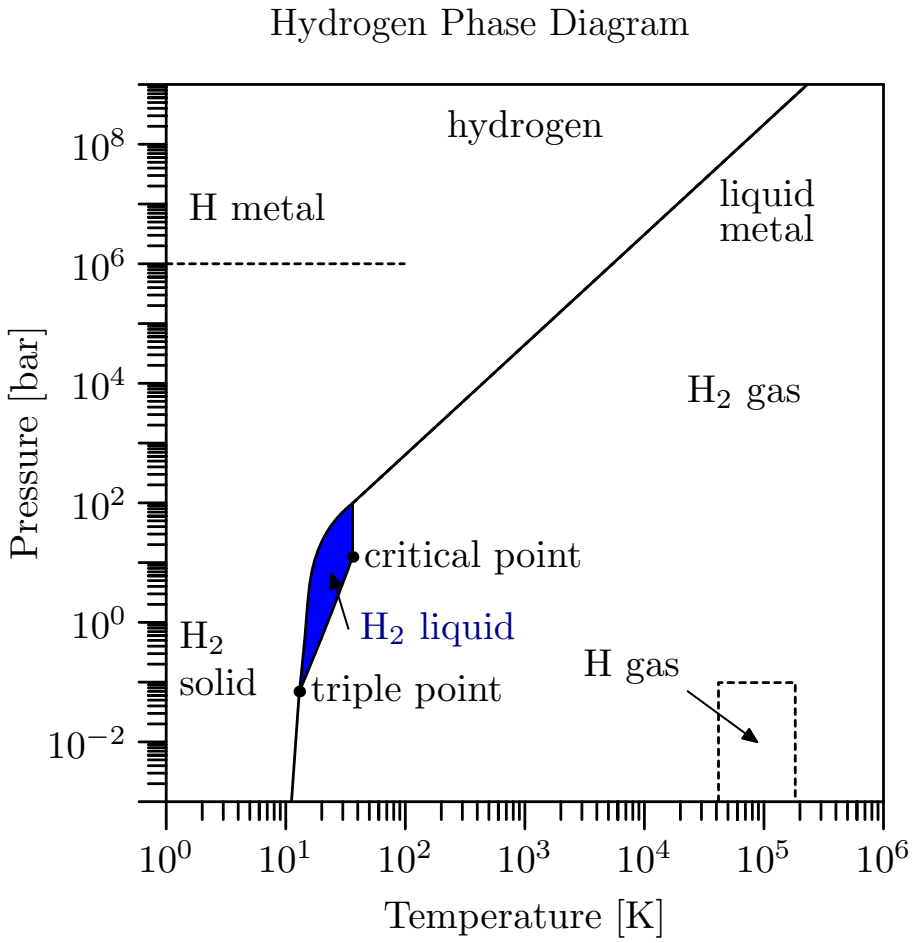
TU Delft

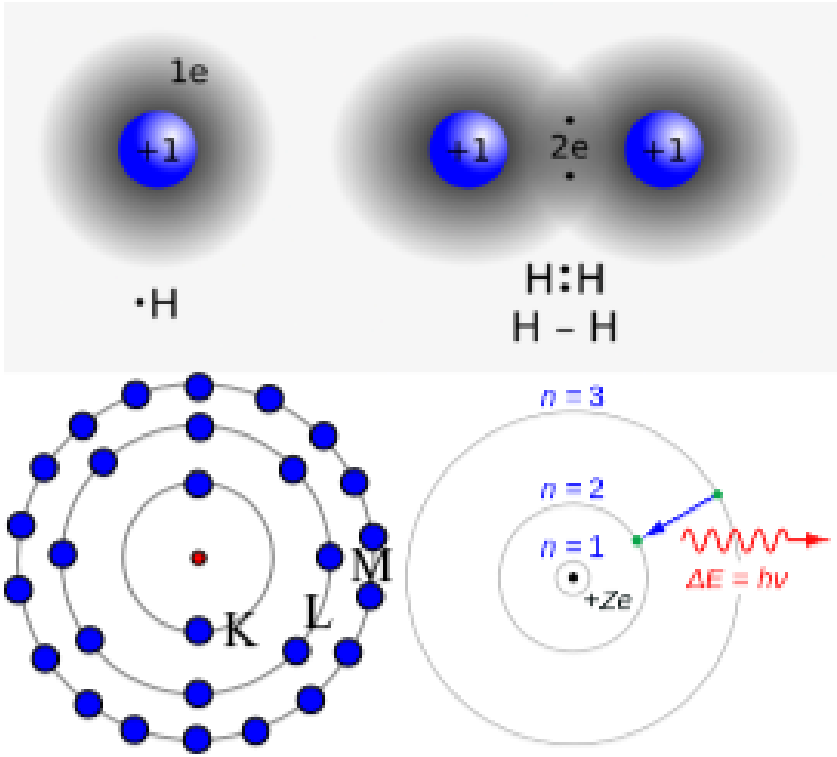
Delft University of Technology



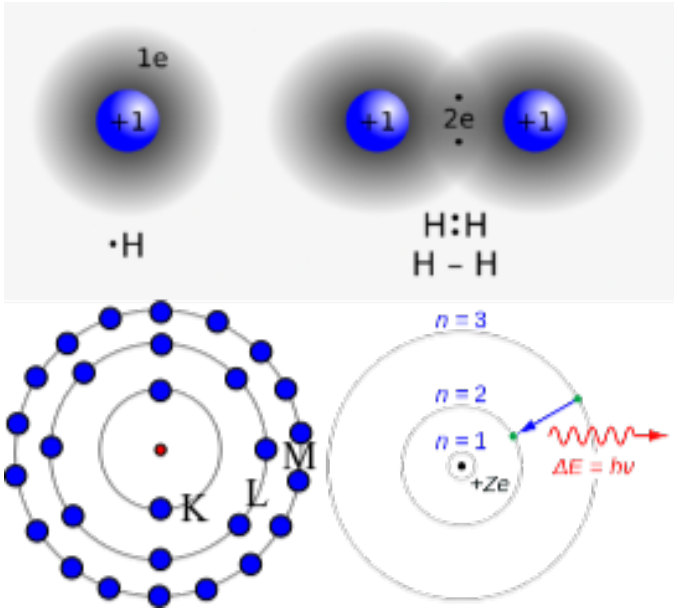
Hydrogen Material Incompatibility: Damage Mechanisms

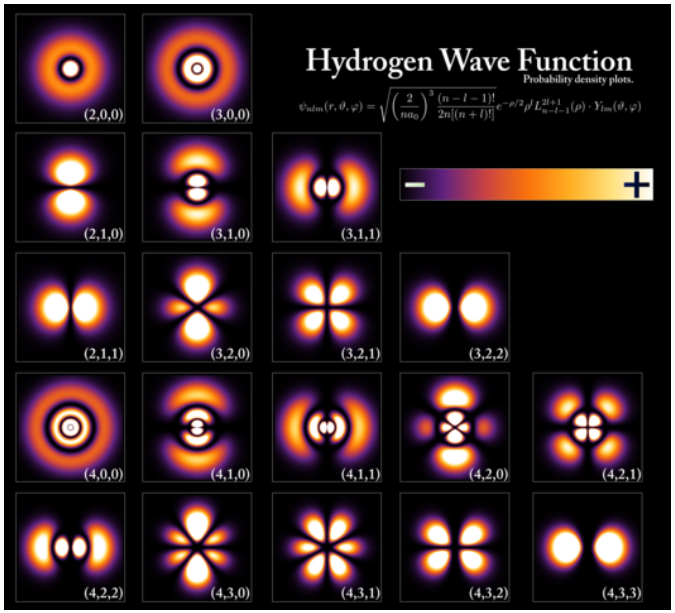
[Dr A.E. Dahoe: *Principles of Hydrogen Safety*, Knowledge Center for Explosion and Hydrogen Safety]





[Dr A.E. Dahoe: *Principles of Hydrogen Safety*, Knowledge Center for Explosion and Hydrogen Safety]

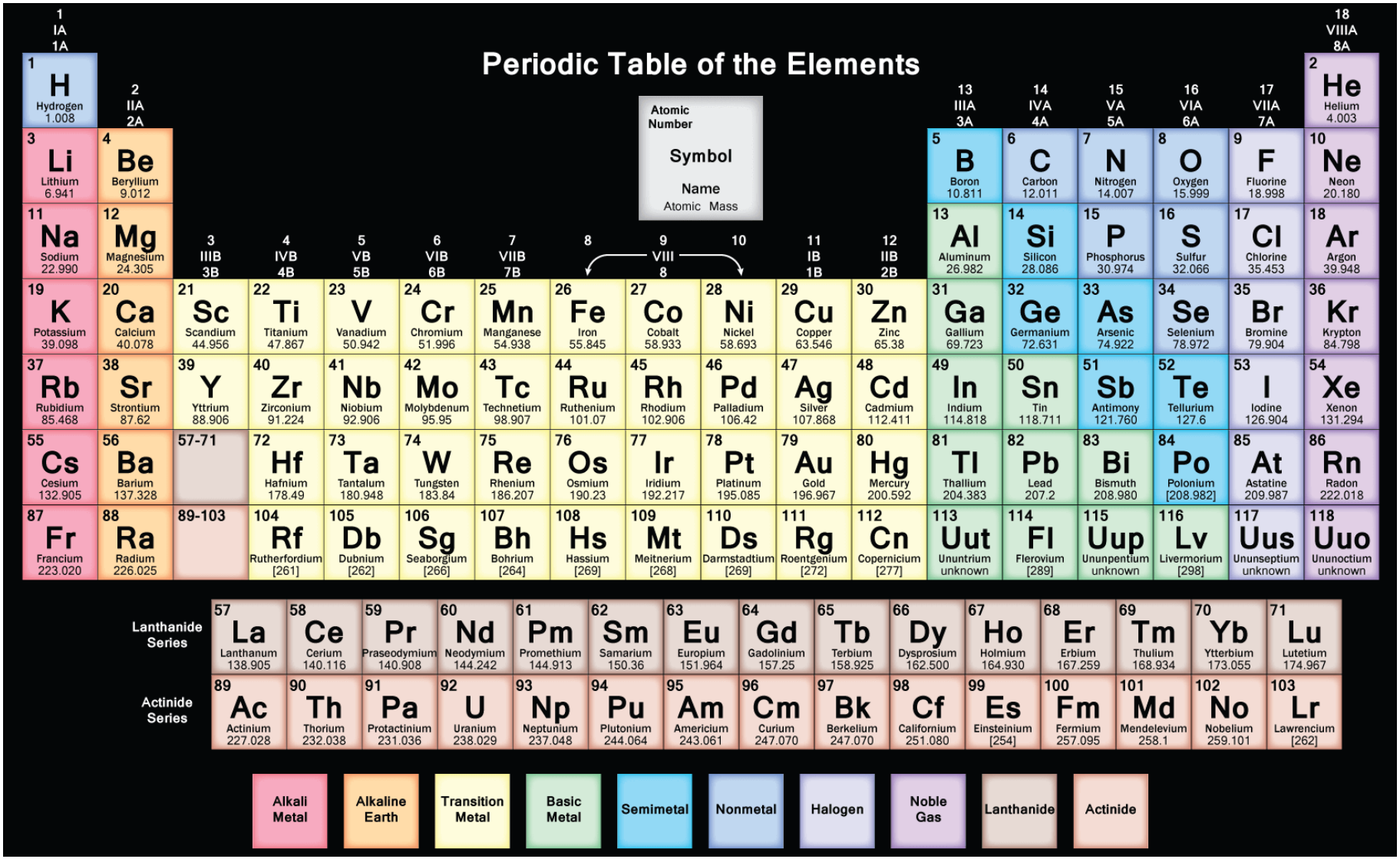




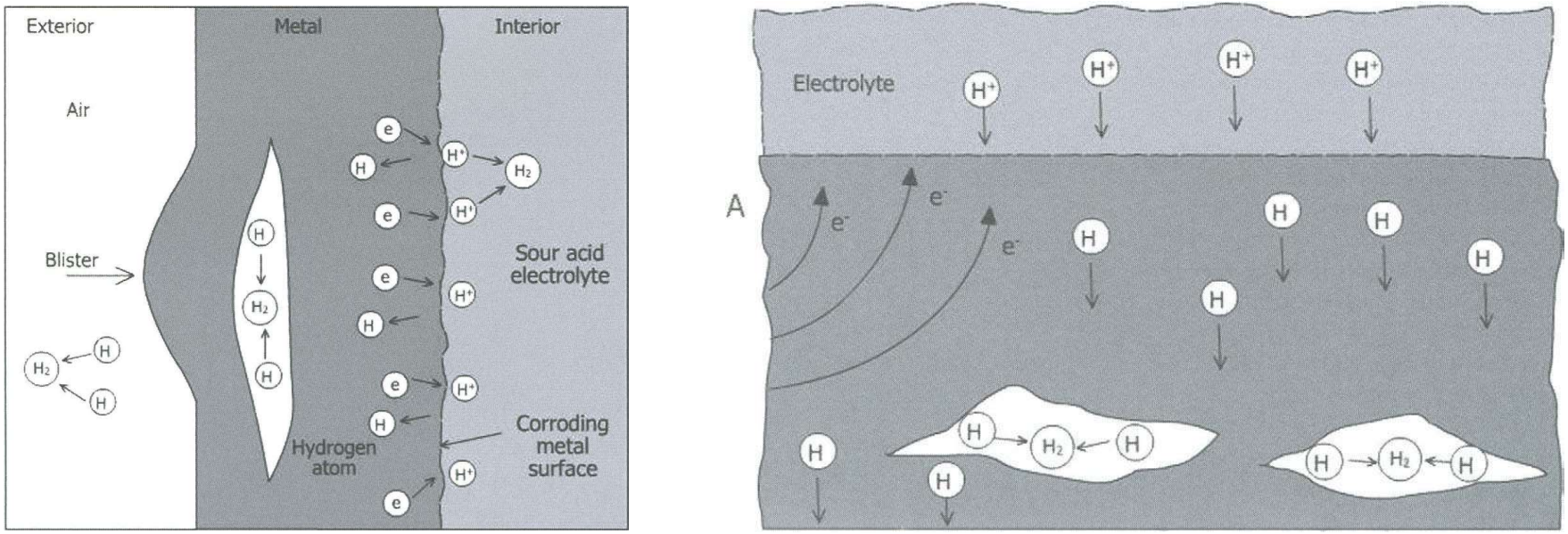
ELECTRONIC STRUCTURE AND CONFIGURATION:

Noble gasses:	**He**: $1s^2$, **Ne**: $1s^2 2s^2 2p^6$, **Ar**: $1s^2 2s^2 2p^6 3s^2 3p^6$, **Kr**: $1s^2 2s^2 2p^6 3s^2 3p^6 4s^2 3d^{10} 4p^6$
Halogens:	**F**: $1s^2 2s^2 2p^5$, **Cl**: $1s^2 2s^2 2p^6 3s^2 3p^5$, **Br**: $1s^2 2s^2 2p^6 3s^2 3p^6 4s^2 3d^{10} 4p^5$
Paramagnetic:	**H**: $1s^1$, **Fe**: $1s^2 2s^2 2p^6 3s^2 3p^6 4s^2 3d^6$, **Ni**: $1s^2 2s^2 2p^6 3s^2 3p^6 4s^2 3d^8$
Diamagnetic:	**Be**: $1s^2 2s^2$, **Hg**: $1s^2 2s^2 2p^6 3s^2 3p^6 4s^2 3d^{10} 4p^6 4d^{10} 5s^2 5p^6 6s^2 4f^{14} 5d^{10}$, **Ag**: $1s^2 2s^2 2p^6 3s^2 3p^6 4s^2 3d^{10} 4p^6 5s^1 4d^{10}$, **Au**: $1s^2 2s^2 2p^6 3s^2 3p^6 4s^2 3d^{10} 4p^6 4d^{10} 5s^2 5p^6 6s^1 4f^{14} 5d^{10}$
Non-magnetic?	**Mn**: $1s^2 2s^2 2p^6 3s^2 3p^6 4s^2 3d^5$, **Cu**: $1s^2 2s^2 2p^6 3s^2 3p^6 4s^1 3d^{10}$

Electron shells are labeled by quantum numbers ($n = 1, 2, 3, \ldots$) or letters (K, L, M, ...) containing a maximum number of $2n^2$ electrons. Subshells are designated by small letters (s, p, d, f, ...) comprising orbitals.


Periodic Table of the Elements
Atomic Number
Symbol
Name
Atomic Mass
1 IA 1A
2 IIA 2A
3 IIIB 3B
4 IVB 4B
5 VB 5B
6 VIB 6B
7 VIIB 7B
8
9 VIII 8
10
11 IB 1B
12 IIB 2B
13 IIIA 3A
14 IVA 4A
15 VA 5A
16 VIA 6A
17 VIIA 7A
18 VIIIA 8A
1 H Hydrogen 1.008
2 He Helium 4.003
3 Li Lithium 6.941
4 Be Beryllium 9.012
5 B Boron 10.811
6 C Carbon 12.011
7 N Nitrogen 14.007
8 O Oxygen 15.999
9 F Fluorine 18.998
10 Ne Neon 20.180
11 Na Sodium 22.990
12 Mg Magnesium 24.305
13 Al Aluminum 26.982
14 Si Silicon 28.086
15 P Phosphorus 30.974
16 S Sulfur 32.066
17 Cl Chlorine 35.453
18 Ar Argon 39.948
19 K Potassium 39.098
20 Ca Calcium 40.078
21 Sc Scandium 44.956
22 Ti Titanium 47.867
23 V Vanadium 50.942
24 Cr Chromium 51.996
25 Mn Manganese 54.938
26 Fe Iron 55.845
27 Co Cobalt 58.933
28 Ni Nickel 58.693
29 Cu Copper 63.546
30 Zn Zinc 65.38
31 Ga Gallium 69.723
32 Ge Germanium 72.631
33 As Arsenic 74.922
34 Se Selenium 78.972
35 Br Bromine 79.904
36 Kr Krypton 84.798
37 Rb Rubidium 85.468
38 Sr Strontium 87.62
39 Y Yttrium 88.906
40 Zr Zirconium 91.224
41 Nb Niobium 92.906
42 Mo Molybdenum 95.95
43 Tc Technetium 98.907
44 Ru Ruthenium 101.07
45 Rh Rhodium 102.906
46 Pd Palladium 106.42
47 Ag Silver 107.868
48 Cd Cadmium 112.411
49 In Indium 114.818
50 Sn Tin 118.711
51 Sb Antimony 121.760
52 Te Tellurium 127.6
53 I Iodine 126.904
54 Xe Xenon 131.294
55 Cs Cesium 132.905
56 Ba Barium 137.328
57-71
72 Hf Hafnium 178.49
73 Ta Tantalum 180.948
74 W Tungsten 183.84
75 Re Rhenium 186.207
76 Os Osmium 190.23
77 Ir Iridium 192.217
78 Pt Platinum 195.085
79 Au Gold 196.967
80 Hg Mercury 200.592
81 Tl Thallium 204.383
82 Pb Lead 207.2
83 Bi Bismuth 208.980
84 Po Polonium [208.982]
85 At Astatine 209.987
86 Rn Radon 222.018
87 Fr Francium 223.020
88 Ra Radium 226.025
89-103
104 Rf Rutherfordium [261]
105 Db Dubnium [262]
106 Sg Seaborgium [266]
107 Bh Bohrium [264]
108 Hs Hassium [269]
109 Mt Meitnerium [268]
110 Ds Darmstadtium [269]
111 Rg Roentgenium [272]
112 Cn Copernicium [277]
113 Uut Ununtrium unknown
114 Fl Flerovium [289]
115 Uup Ununpentium unknown
116 Lv Livermorium [298]
117 Uus Ununseptium unknown
118 Uuo Ununoctium unknown
Lanthanide Series
57 La Lanthanum 138.905
58 Ce Cerium 140.116
59 Pr Praseodymium 140.908
60 Nd Neodymium 144.242
61 Pm Promethium 144.913
62 Sm Samarium 150.36
63 Eu Europium 151.964
64 Gd Gadolinium 157.25
65 Tb Terbium 158.925
66 Dy Dysprosium 162.500
67 Ho Holmium 164.930
68 Er Erbium 167.259
69 Tm Thulium 168.934
70 Yb Ytterbium 173.055
71 Lu Lutetium 174.967
Actinide Series
89 Ac Actinium 227.028
90 Th Thorium 232.038
91 Pa Protactinium 231.036
92 U Uranium 238.029
93 Np Neptunium 237.048
94 Pu Plutonium 244.064
95 Am Americium 243.061
96 Cm Curium 247.070
97 Bk Berkelium 247.070
98 Cf Californium 251.080
99 Es Einsteinium [254]
100 Fm Fermium 257.095
101 Md Mendelevium 258.1
102 No Nobelium 259.101
103 Lr Lawrencium [262]
Alkali Metal
Alkaline Earth
Transition Metal
Basic Metal
Semimetal
Nonmetal
Halogen
Noble Gas
Lanthanide
Actinide

INTERNAL HYDROGEN EMBRITTLEMENT

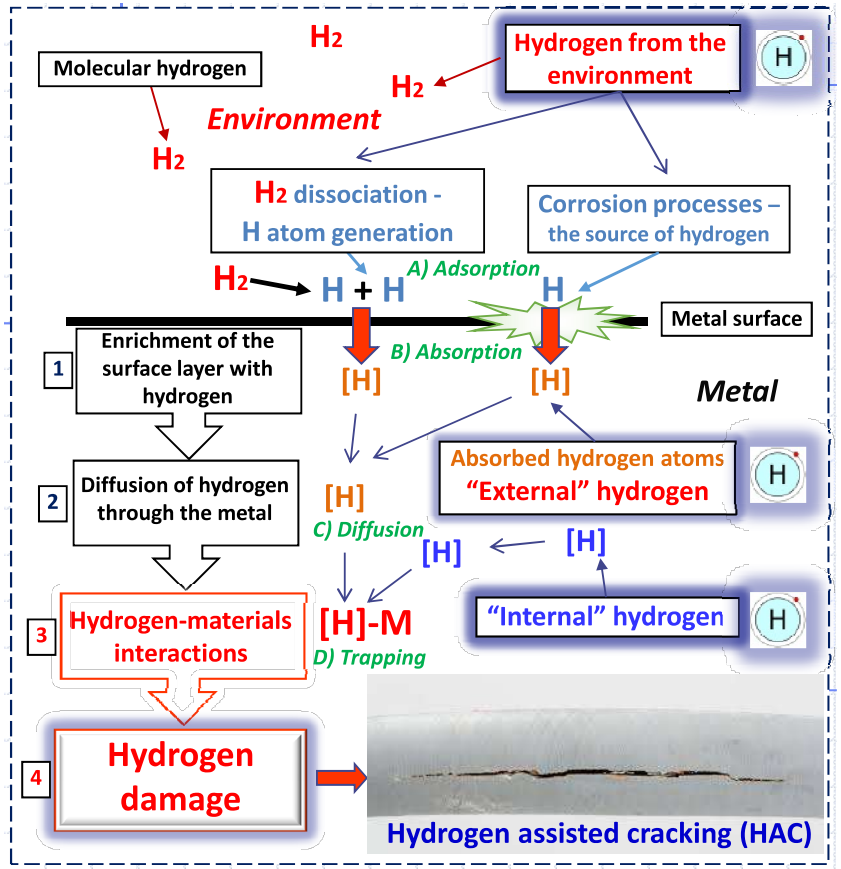


Internal Hydrogen Embrittlement [1]: Blistering.

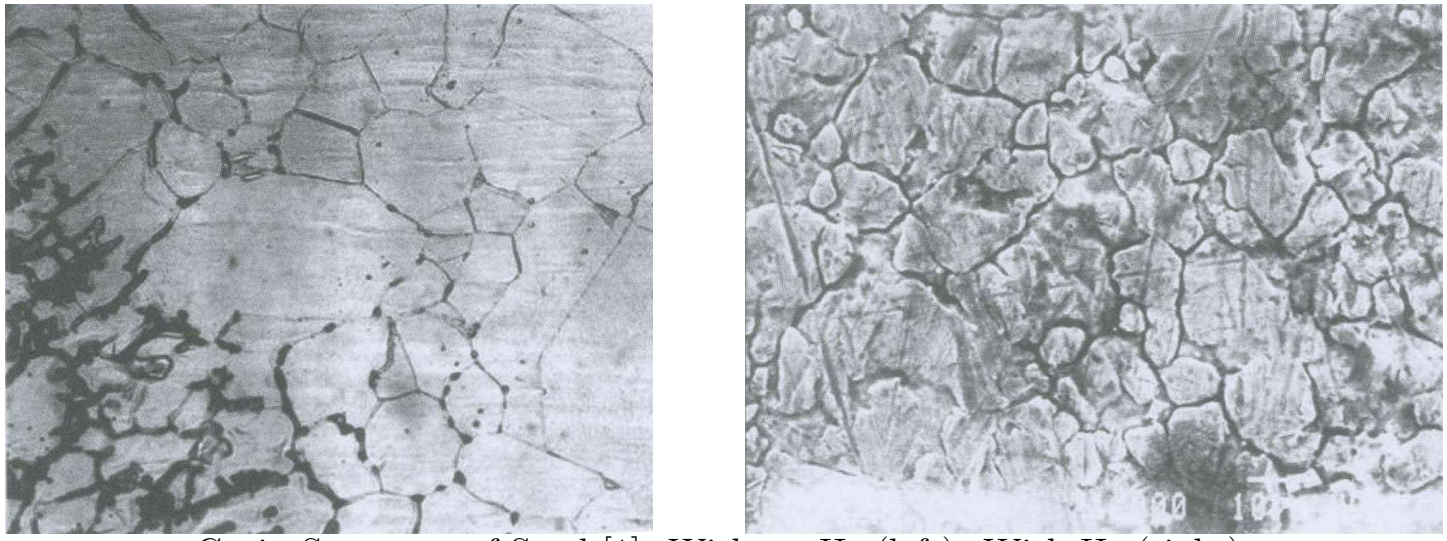
Interior:	$\mathrm{HCl(g) + H_2O(l) \longrightarrow H_3O^+(aq) + Cl^-(aq)}$	Environmental Hydrogen Embrittlement:
	$\mathrm{2\,H_3O^+(aq) + 2\,e^- \longrightarrow H_2(g) + 2\,H_2O(l)}$	$\mathrm{2\,H_2O(l) \longrightarrow H_3O^+(aq) + OH^-(aq)}$
Metal:	$\mathrm{M(s) - \beta e^- + \beta Cl^-(aq) \longrightarrow MCl_\beta(s)}$ [surface]	$\mathrm{2\,H_3O^+(aq) + 2\,e^- \longrightarrow H_2(g) + 2\,H_2O(l)}$
	$\mathrm{\beta H_3O^+(aq) + \beta e^- \longrightarrow \beta H\cdot + \beta H_2O(l)}$ [surface]	$\mathrm{M(s) - \beta e^- + \beta OH^-(aq) \longrightarrow M[OH]_\beta(s)}$
	$\mathrm{H\cdot + H\cdot \longrightarrow H_2(g)}$ [bulk]	$\mathrm{\beta H_3O^+(aq) + \beta e^- \longrightarrow \beta H\cdot + \beta H_2O(l)}$
Exterior:	$\mathrm{H\cdot + H\cdot \longrightarrow H_2(g)}$	$\mathrm{H\cdot + H\cdot \longrightarrow H_2(g)}$
		Construction elements of bridges

HYDROGEN ENRICHMENT OF METAL

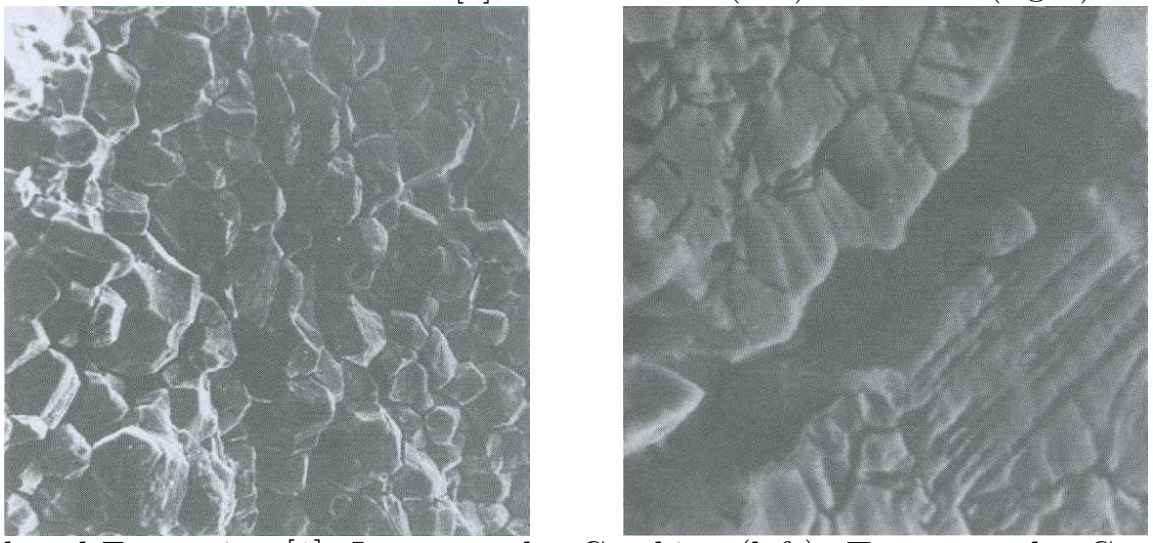
HYDROGEN DAMAGE MECHANISMS [2]



- Hydrogen Embrittlement (HE), Hydrogen-Induced Cracking (HIC) and High-Temperature Hydrogen Attack (HTHA) of low carbon and low alloy steel pipelines, pressure vessels, and tubes in the power and oil and gas industry
- HE of high-strength (titanium) and other high-toughness alloys, including high strength steels, and aluminum alloys used in military aircraft and other equipment
- HE of nickel-based alloys and failure of duplex stainless steels for subsea applications in critical components exposed to seawater and other equipment
- Hydrogen-induced fractures and HE of martensitic and other advanced high strength steels used by automotive manufacturers to create lightweight, crashworthy cars
- HE of precipitation-hardened high-strength steels and copper-based alloys for use in hydrogen refueling stations
- HE and HIC of fasteners in marine and other aggressive environments; and Hydride Embrittlement of metallic alloys for nuclear systems



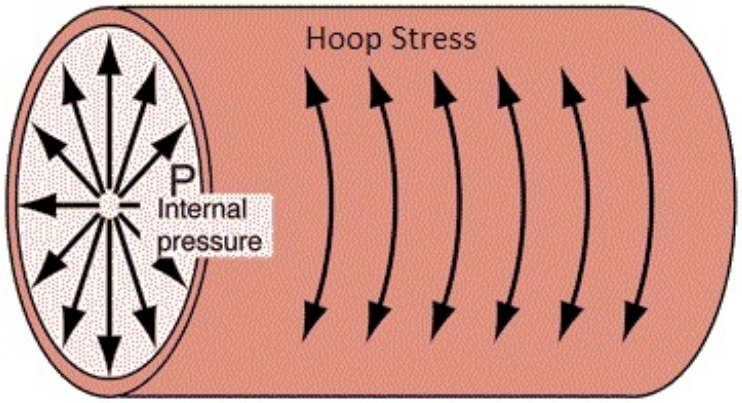
Grain Structure of Steel [1]. Without H_2 (left). With H_2 (right).



Hydrogen Induced Fracturing [1]. Intergranular Cracking (left). Transgranular Cracking (right).

$$H_2 \underset{k_b}{\overset{k_f}{\rightleftharpoons}} H\cdot + H\cdot \qquad K_{eq}(P,T) = \frac{k_f}{k_b} = \frac{p^2_{H\cdot}}{p_{H_2}}$$

$$H\cdot \xrightarrow{\text{diffusion}} \text{Metal}$$

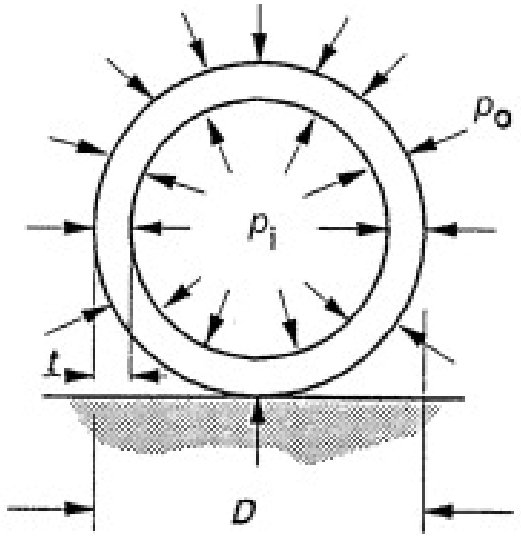


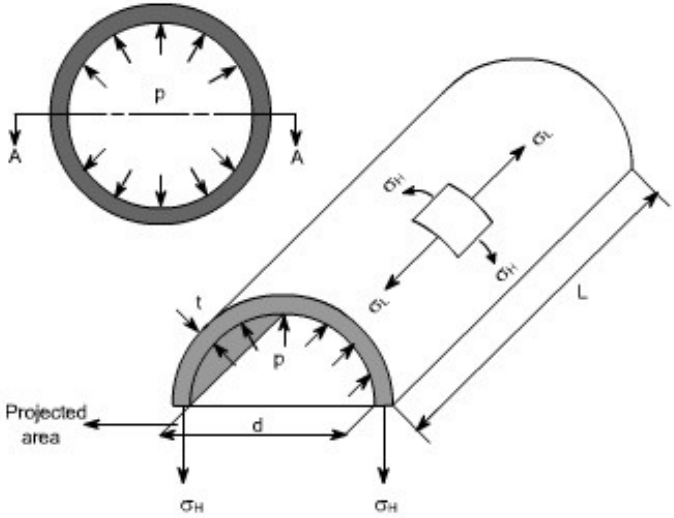
Hoop Stress and Longitudinal Stress

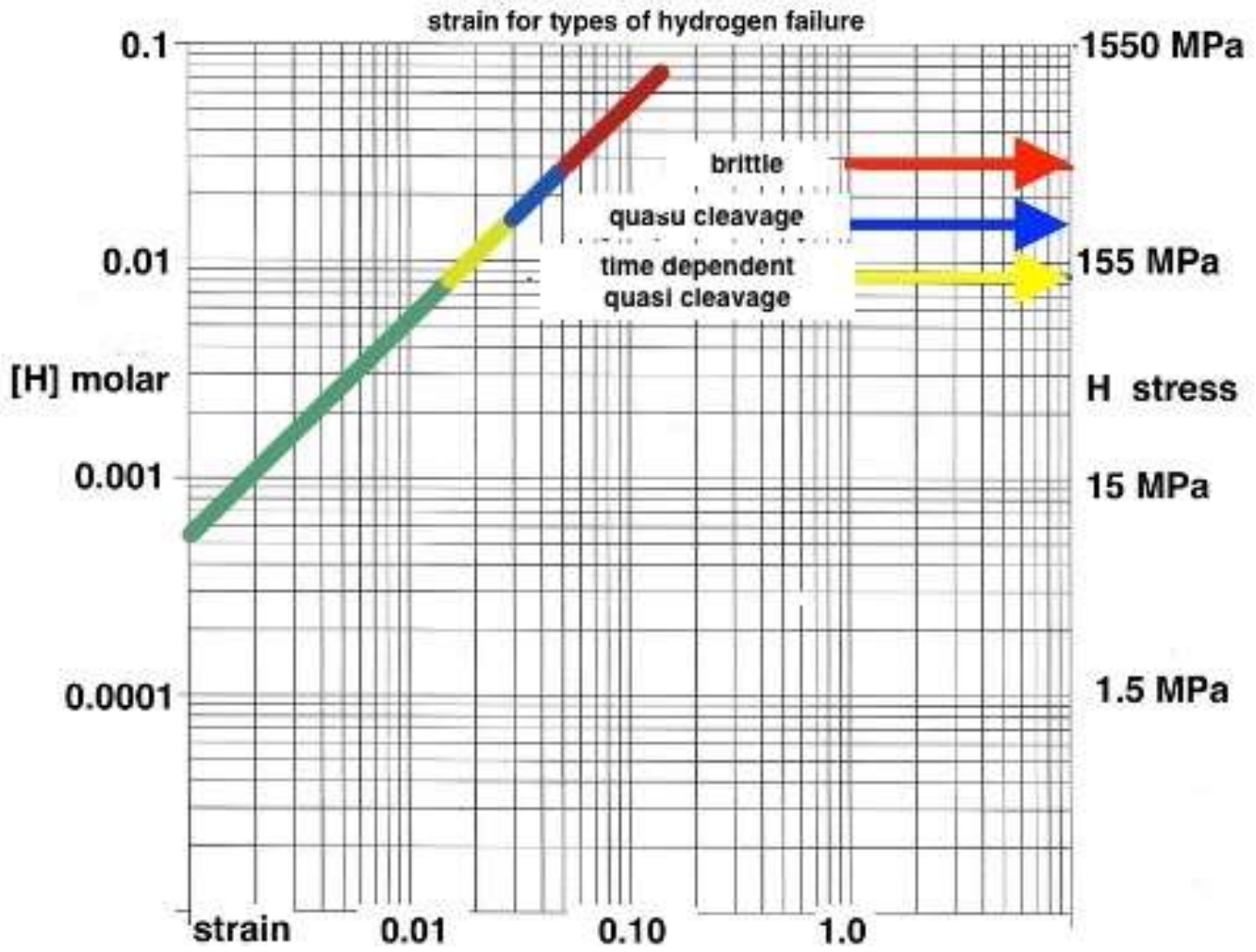


Hoop stress

$$\sigma_h = \frac{(p_i - p_o)D}{2t}$$



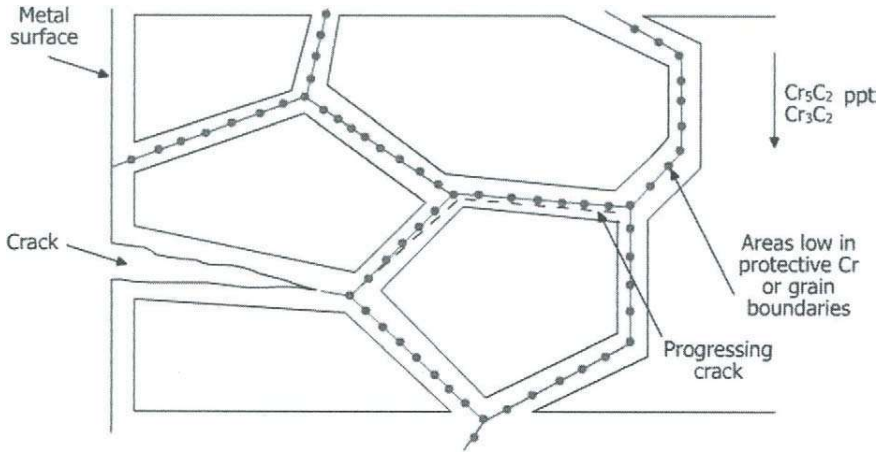




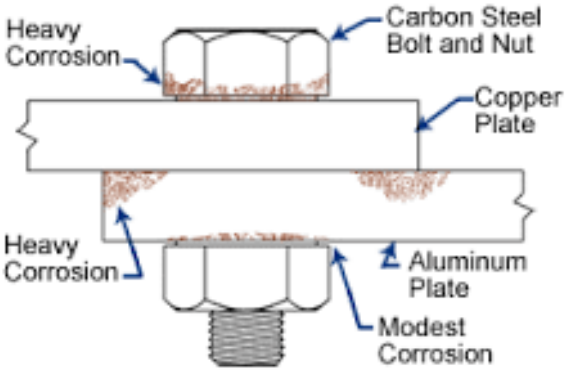
Hydrogen Concentration – Stress - Strain Diagram (700 MPa yield strength steel) [3]

$$H_2 \underset{k_b}{\overset{k_f}{\rightleftharpoons}} H\cdot + H\cdot \qquad K_{eq}(P,T) = \frac{k_f}{k_b} = \frac{p^2_{H\cdot}}{p_{H_2}}$$

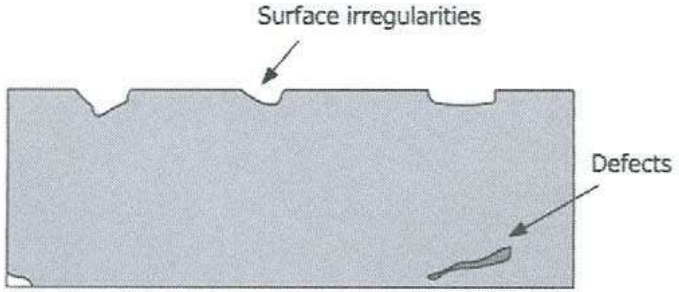
$H\cdot \xrightarrow{\text{diffusion}}$ Metal

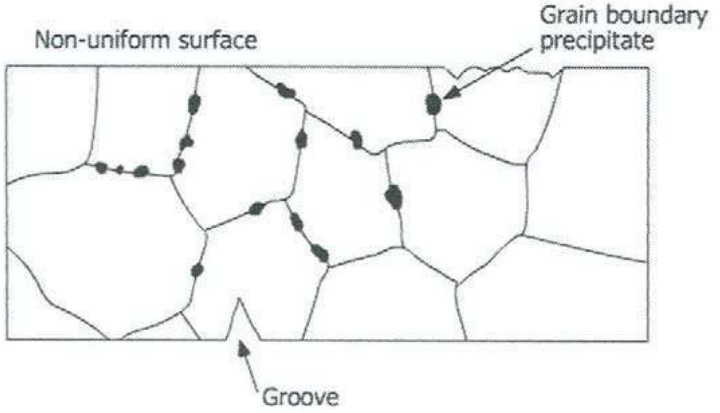


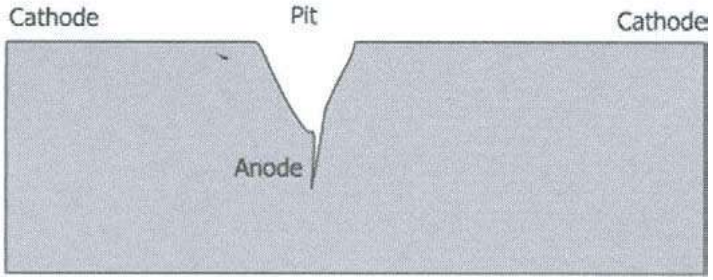
Intergranular Stress Assisted Cracking [1]:
Fracture Propagation Along Grain Boundaries
Galvanic (Anodic/Cathodic) Protection Required



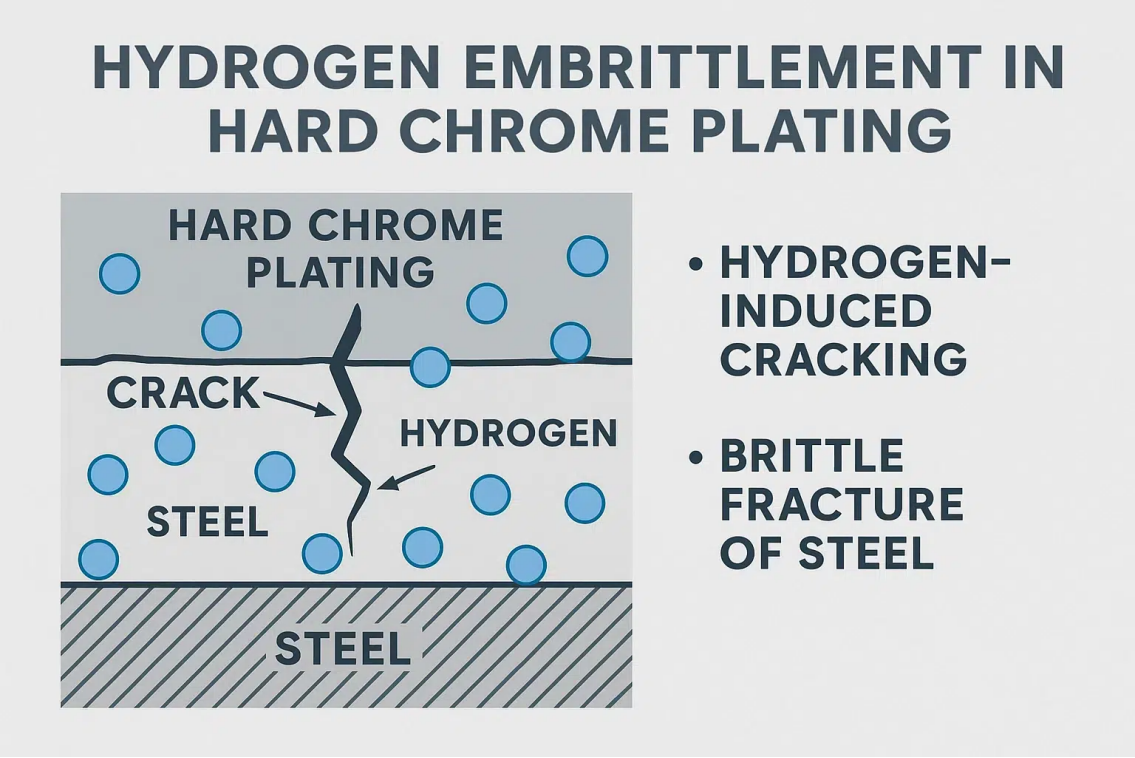
Effects of Galvanic Corrosion

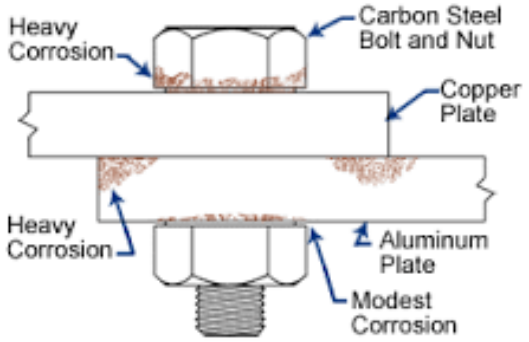






PROTECTING STEEL FROM GALVANIC CORROSION – CHROME PLATING

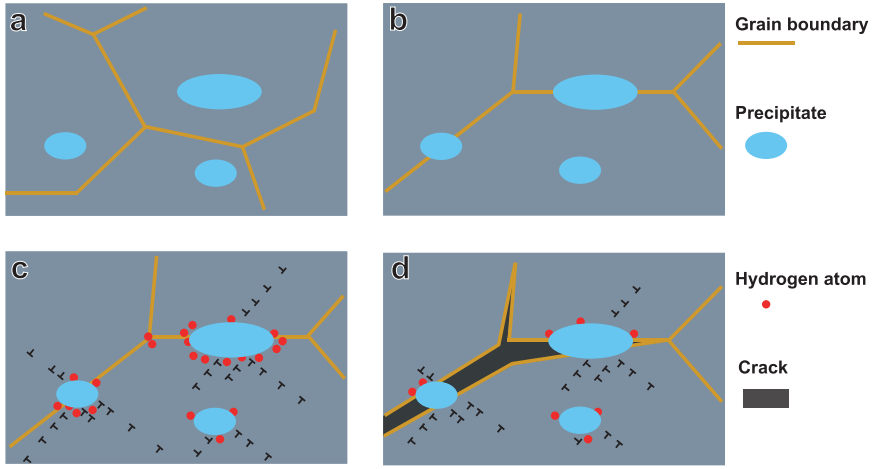




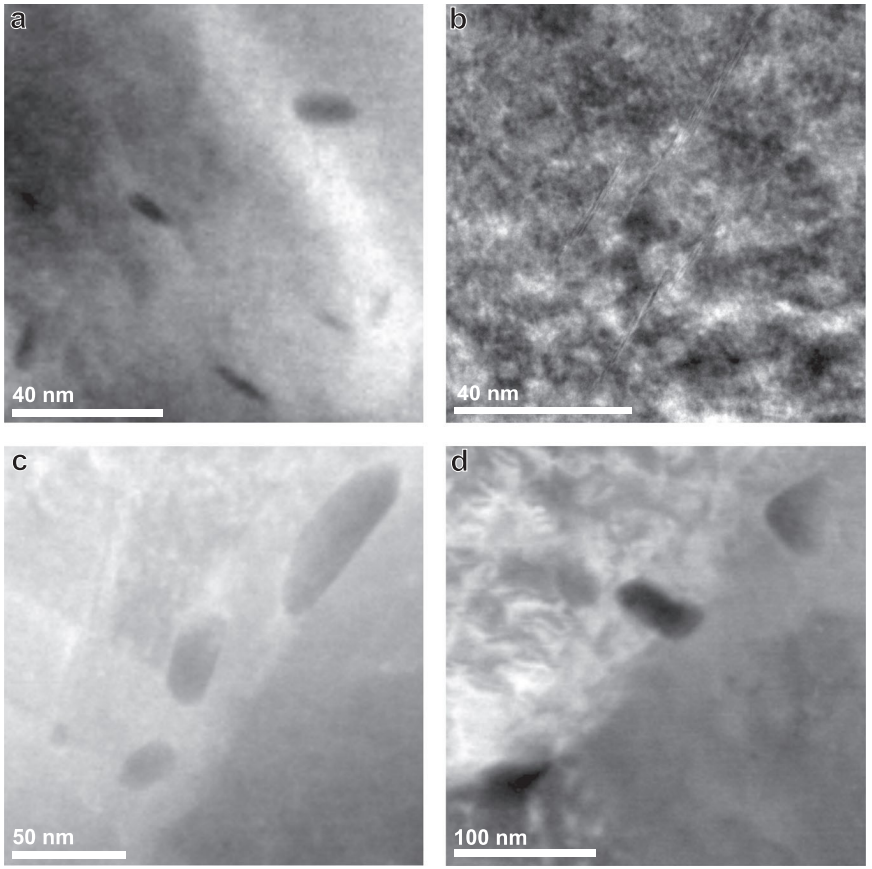
Effects of Galvanic Corrosion

Effect of hydrogen on chrome plated steel

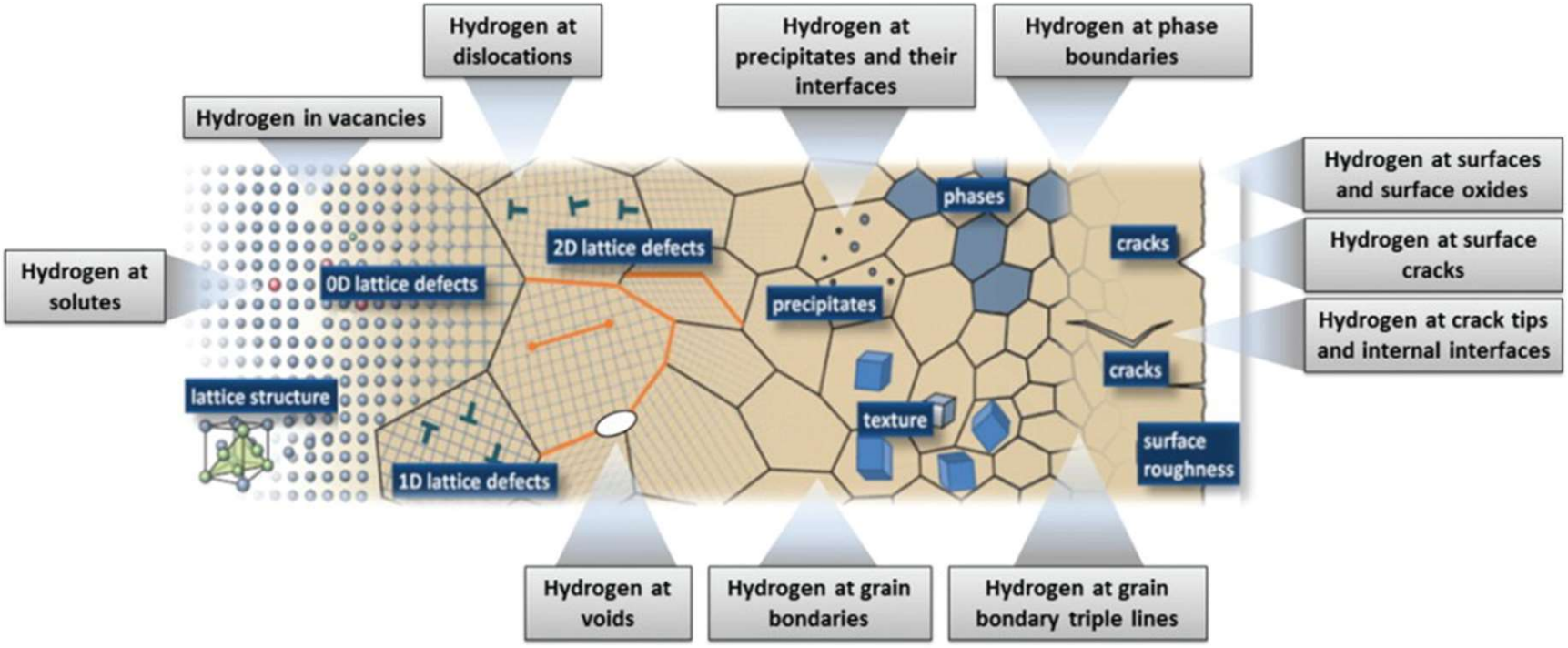
Alloy type	C	Mn	Al	Si	Ti	V	Trace elements	Balance Fe
TiC	0.07	1.7	0.01	0.01	0.30	–	0.04	97.8
VC	0.07	1.8	0.01	0.02	–	0.31	0.03	97.8



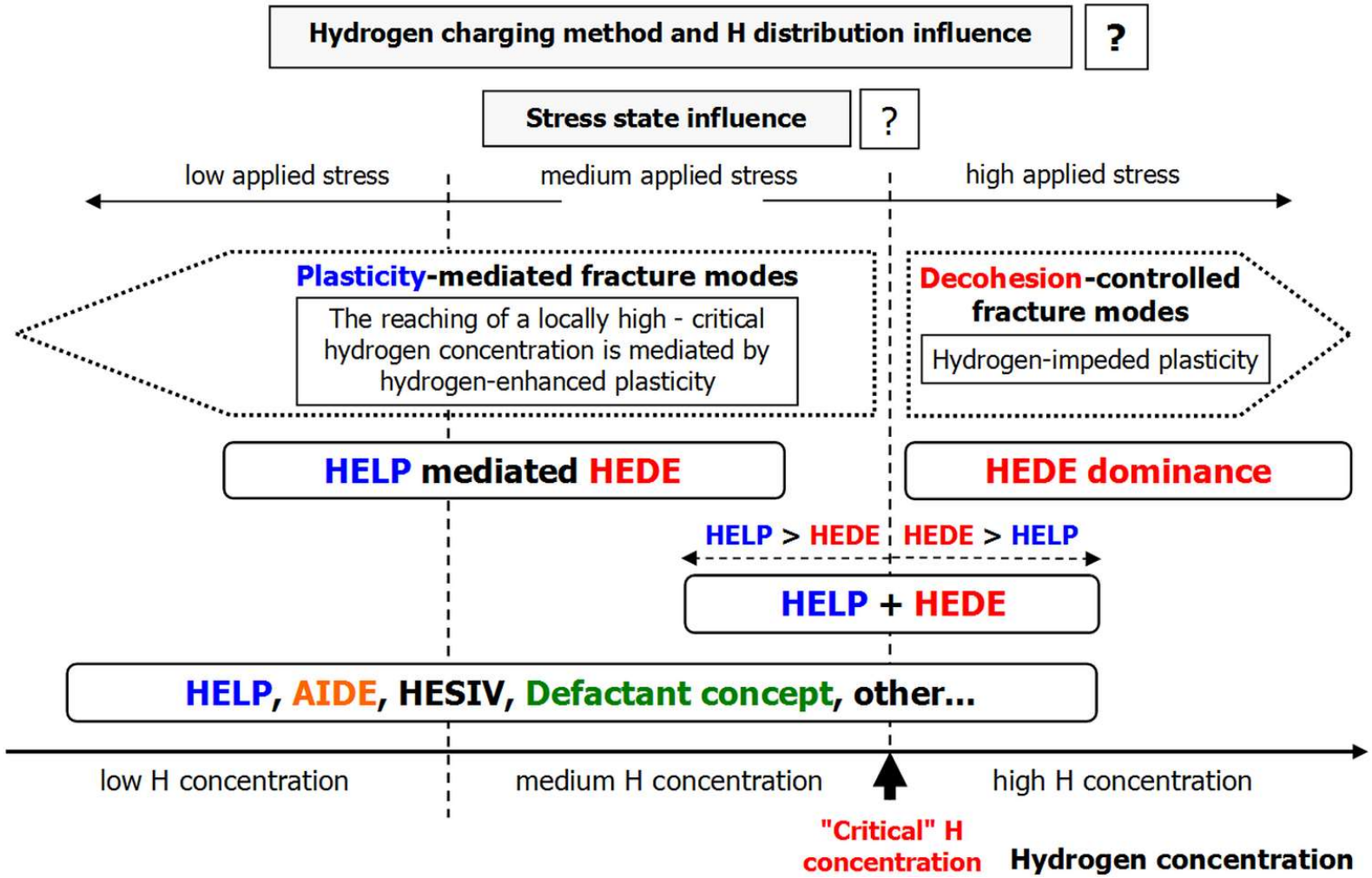
Hydrogen trapping by titanium carbide and vanadium carbide precipitates [4].



Hydrogen trapping by carbide precipitates [4]: (a) titanium carbide, (b) vanadium carbide, (c) titanium carbide, (d) vanadium carbide.



Hydrogen trapping sites in steels [5, 6].



Unified model for synergistic hydrogen embrittlement mechanisms in steels [5].

STEEL COMPOSITIONS

Type	Fe	C	Cr	Ni	Mn	Mo	Si	N	S	P	Nb	Ti	V	Al	Cu	B	Sn	Ca
	wt%	wt%	wt%	wt%	wt%	wt%	wt%	wt%	wt%	wt%	wt%	wt%	wt%	wt%	wt%	wt%	wt%	wt%
316	bulk	0.08	16-18	10-14	2	2-3	1		0.030-0.045	0.030-0.045								
316L	bulk	0.03	16-18	10-14	2	2-3	1		0.030-0.045	0.030-0.045								
X<number> stands for pipeline steel in the API standard. The **<number>** denotes the strength level in *kpsi* units. Example: **X70** represents pipeline steel with a minimum yield strength of 70 kpsi.																		
X42	bulk	0.22		0.30	1.30	0.15	0.45		0.015	0.025	0.05	0.04	0.05		0.50			
X52	bulk	0.16			1.60		0.15	0.014	0.007	0.025	0.04	0.02	0.06	0.06	0.30	0.0005	0.02	
X60	bulk	0.16			1.65		0.45		0.010	0.020	0.05	0.04	0.08					
X65	bulk	0.16			1.65		0.45		0.010	0.020	0.05	0.06	0.09					
X70	bulk	0.17			1.75		0.45		0.010	0.020	0.05	0.06	0.10					
X80	bulk	0.03	0.161	0.014	1.76	0.189	0.21	0.0065	0.004	0.016	0.069	0.015	0.025	0.029	0.01	0.0001		0.003
304L	bulk	0.07	17.50-19.50		2.00		1.00		0.015	0.045								
A106	bulk	0.30-0.35			0.29-1.06		0.1		0.035	0.035								
Duplex 1.4462 / UNS S31803 / F51 / X2CrNiMoN22-5-3																		
Min.	bulk		21.0	4.5		2.5		0.10										
max.	bulk	0.03	23.0	6.5	2.0	3.5	1.0	0.22	0.02	0.035								

Additional refererences: [6–11].

EFFECT OF ALLOYING ELEMENTS

TECHNICAL TERMS

Sensitization. When steels, such as austenitic type, are slowly cooled through the range 550 – 850 °C, they frequently become susceptible to intergranular attack in a corrosive medium.
(1) Sensitization occurs only in the temperature range 550 – 850 °C because of the diffusion of the carbon to the grain boundaries.
(2) Fast cooling rate through the sensitizing temperature range does not provide adequate time for the process of sensitizing to occur.
(3) The degree of sensitization increases with increasing carbon content and decreasing chromium content.
(4) Chromium carbide precipitates at the grain boundary. A single carbon atom can tie up almost four chromium atoms.

Stabilized steel. Steels containing stabilizers, such as titanium and niobium, which form carbides that are more stable than chromium carbides, are called stabilized stainless steels.

Chromium depletion. When the concentration of chromium adjacent to the grain boundaries becomes less compared to its concentration away from the grain boundaries, the phenomenon is termed chromium depletion.

Annealing. Slow cooling in the furnace.

Nickel. Decreases susceptibility to sensitization. Because carbon solubility decreases with increased Ni content.

Molybdenum. The susceptibility of steels to intergranular attack decreases with increased Mo content. Mo also increases the resistance to pitting and crevice corrosion.

Chromium. Generally increases the resistance to sensitization.

Nitrogen. The effect of nitrogen depends upon the amount. N is an austenite stabilizer. Steels containing 18% Cr, 9 – 12% Ni and N which are sensitized at 500 °C for 100 h showed a maximum sensitization resistance at 0.04% N.

Titanium and Niobium. Provide stabilization against harmful precipitates (chromium carbides). They combine with C and N. To prohibit C and N to precipitate as carbides and nitrides which lead to intergranular fracturing.

Silicon. Increases corrosion resistance in sulfuric acid.

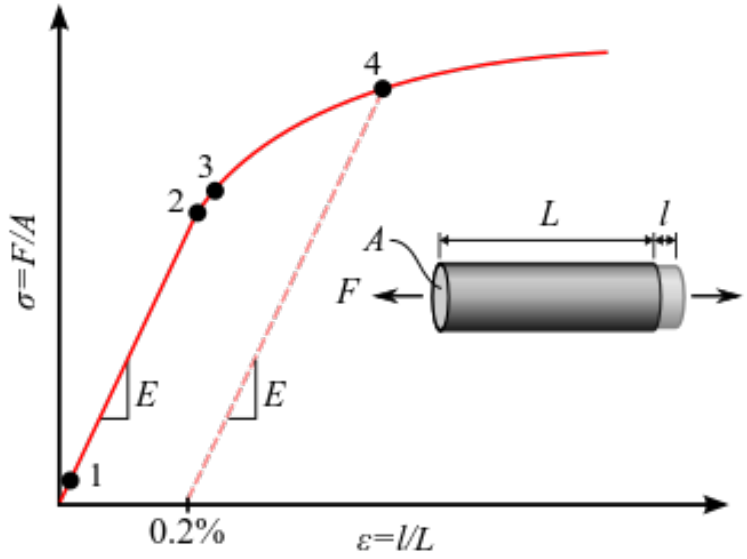
Sulfur and Selenium. Added to increase machinability and malleability. However, corrosion resistance is decreased.

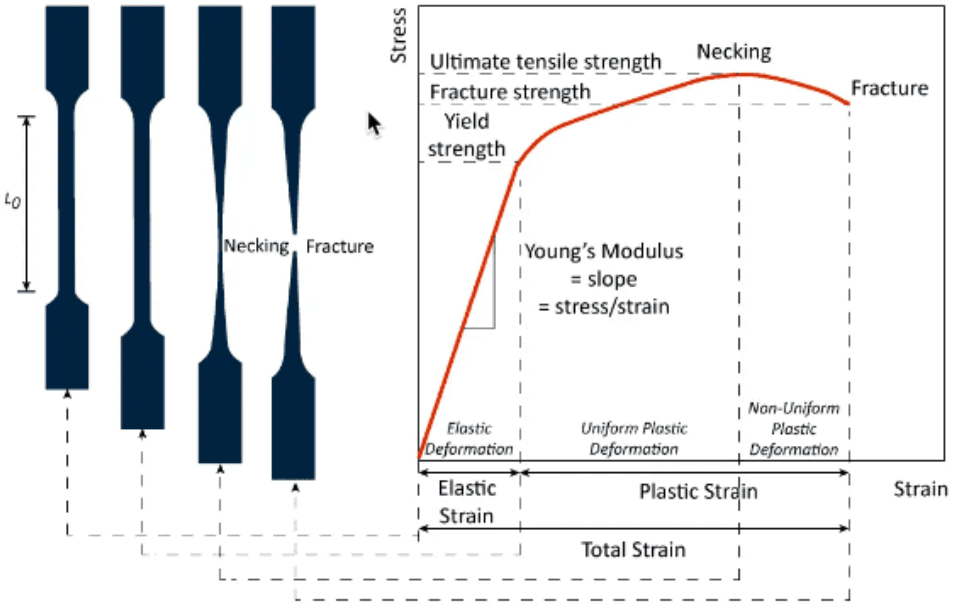
MELT POINTS AND BOILING POINTS OF ELEMENTS

Element	Melt Point (°C)	Boiling Point (°C)
Fe	1538	2862
C	3550	4827
Cr	1907	2671
Ni	1455	2913
Mn	1246	2061
Mo	2623	4639
Si	1410 – 1414	2355 – 3265
N	-210	-196
S	115	444.6
P (white)	44.1	280.5
P (red)	590	–
Nb	2468 – 2477	4742 – 4744
Ti	1668	3287
V	1910	3407
Al	660.32	2470
Cu	1083 – 1085	2562 – 2595
B	2076 – 2350	3927 – 4273
Sn	232	2602
Ca	842	1484

Alloy (Steel)	Melt Point (°C)
AISI 316	1370 – 1400
AISI 316L	1375 – 1400
AISI 304L	1400 – 1450
X42	1420 – 1500
X52	1425 – 1540
X60	1450 – 1520
X65	1370 – 1530
X70	1370 – 1530
X80	1450 – 1500

STRESS-STRAIN CURVE





Stress-Strain Curve:

(1) True elastic limit: the lowest stress at which dislocation movement begins.

(2) Proportionality limit: maximum value where stress is directly proportional to strain.

(3) Elastic limit: permanent deformation occurs.

(4) Offset yield strength: plastic deformation begins to occur.

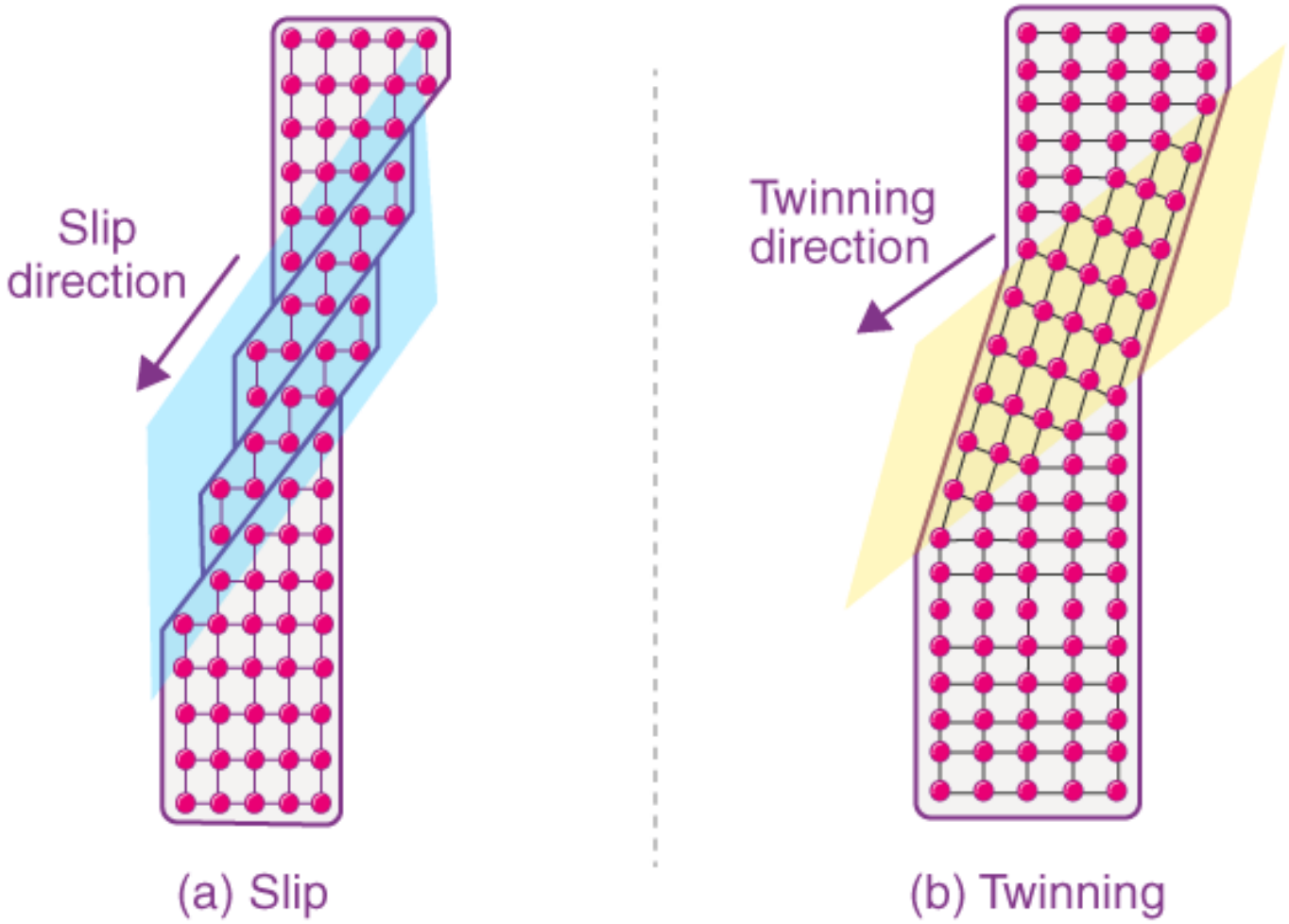
Hydrogen Embrittlement Index (HEI):

$$\epsilon = \frac{\Delta \ell}{\ell} \quad \Longrightarrow \quad \text{HEI 1} = \frac{\epsilon^*}{\epsilon}$$

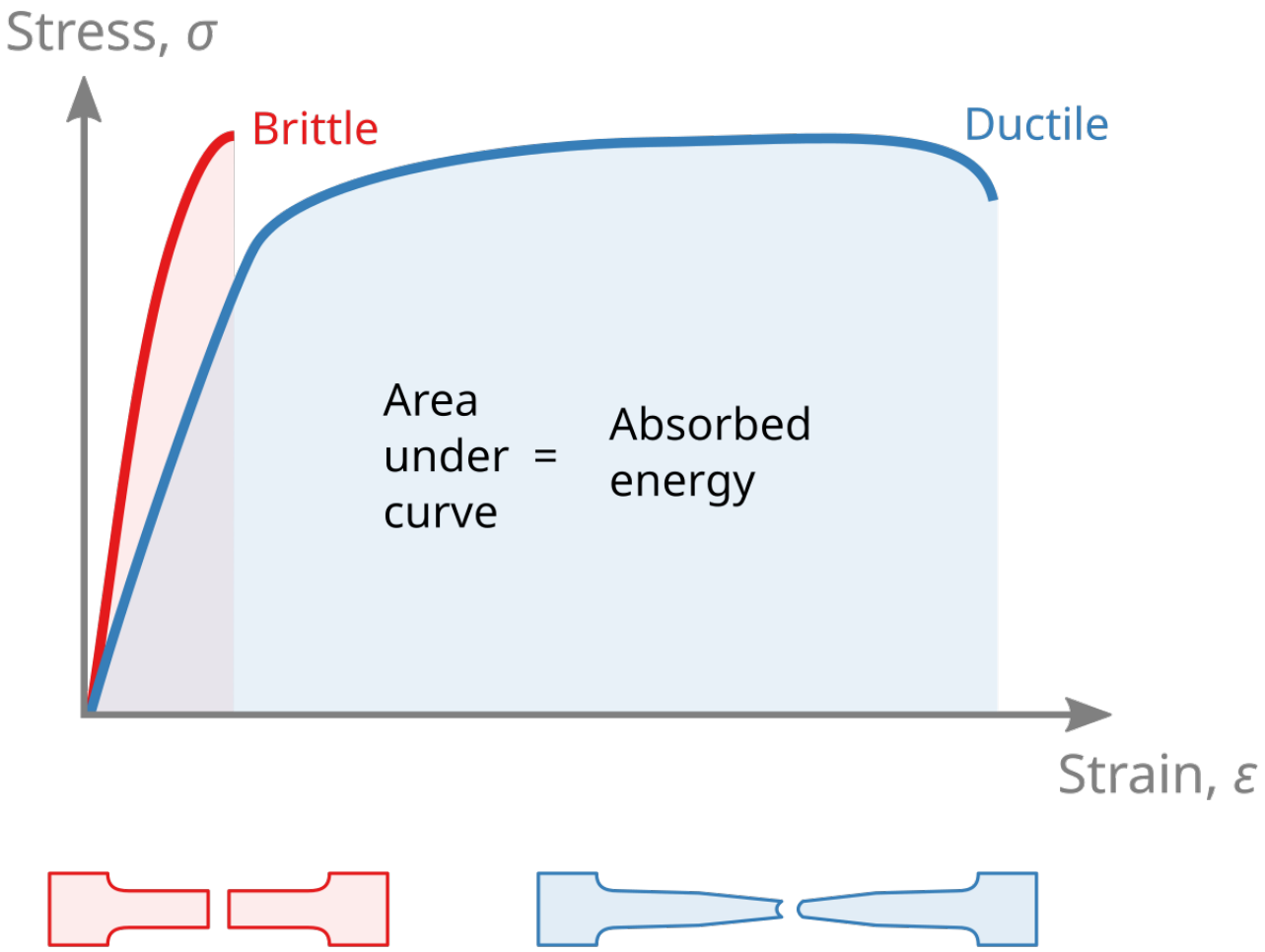
$$\alpha = \frac{\Delta a}{a} \quad \Longrightarrow \quad \text{HEI 2} = \frac{\alpha^*}{\alpha}$$

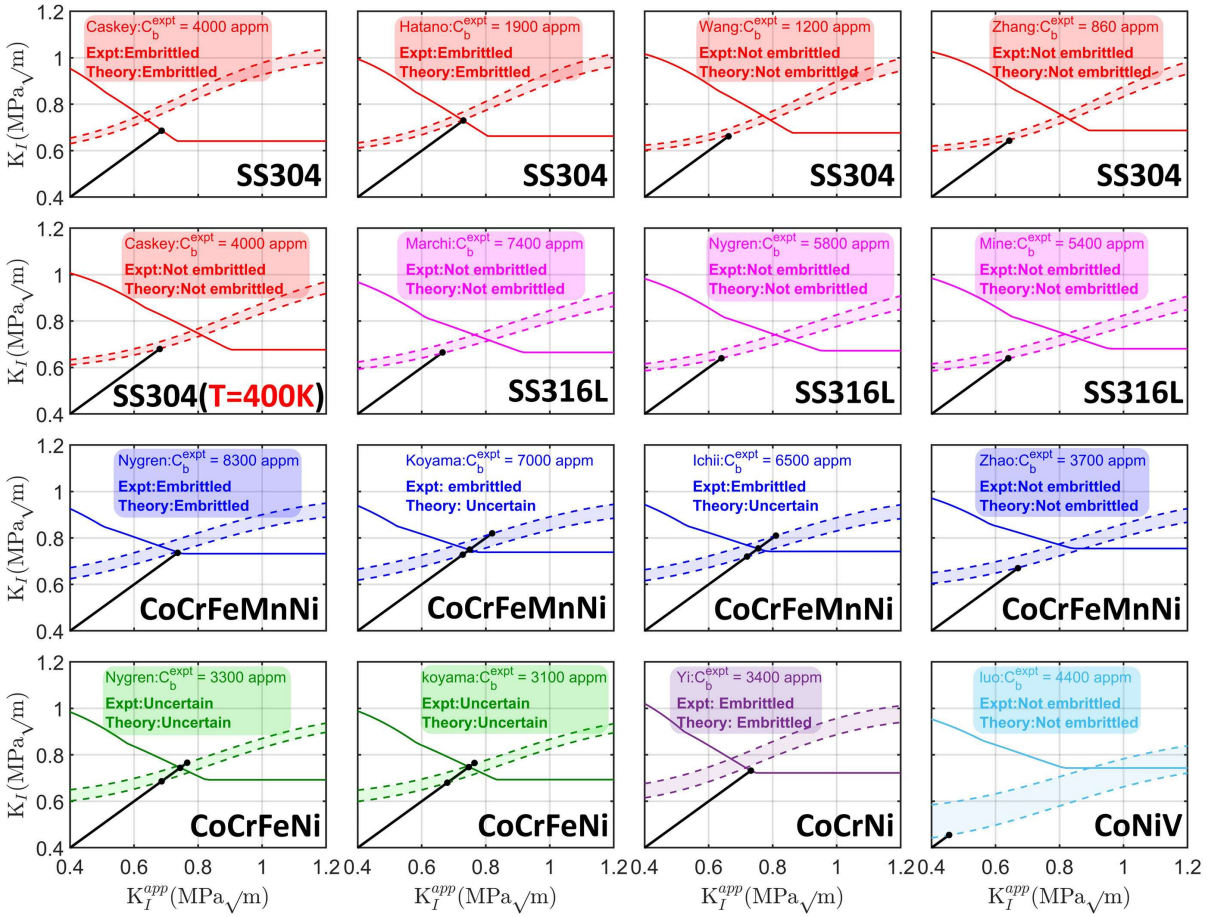
The asterisk ($*$) denotes hydrogen charged.

STRESS-STRAIN CURVE: DISLOCATION



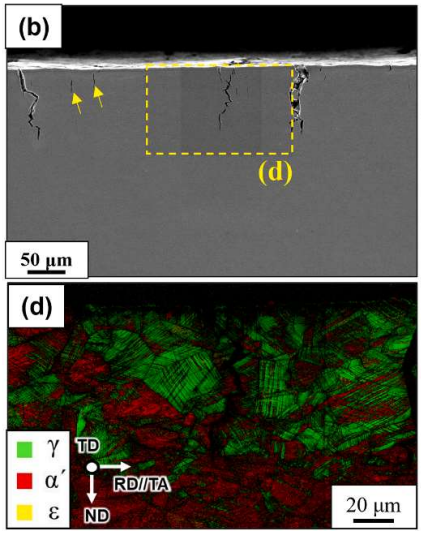
STRESS-STRAIN CURVE: HYDROGEN EMBRITTLEMENT



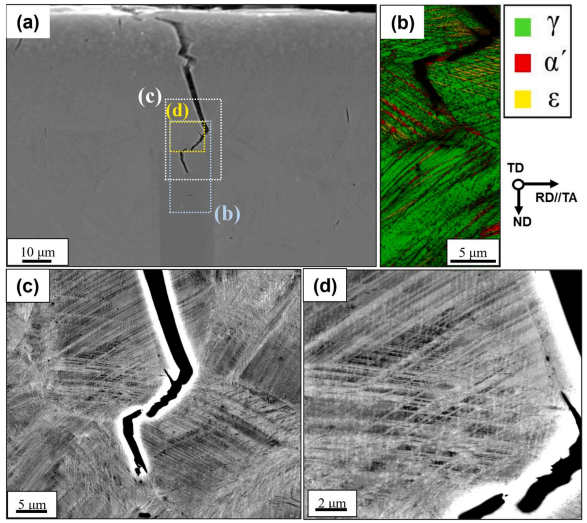


Hydrogen compatibility of various alloys [12]. All experiments, except one, were conducted at 300 K.

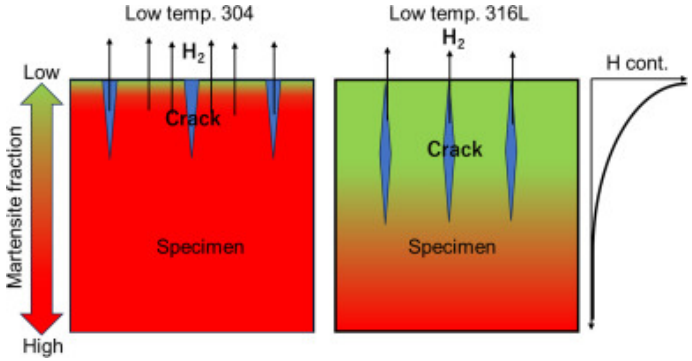
MARTENSITE TRANSFORMATION INDUCED HYDROGEN CRACKING



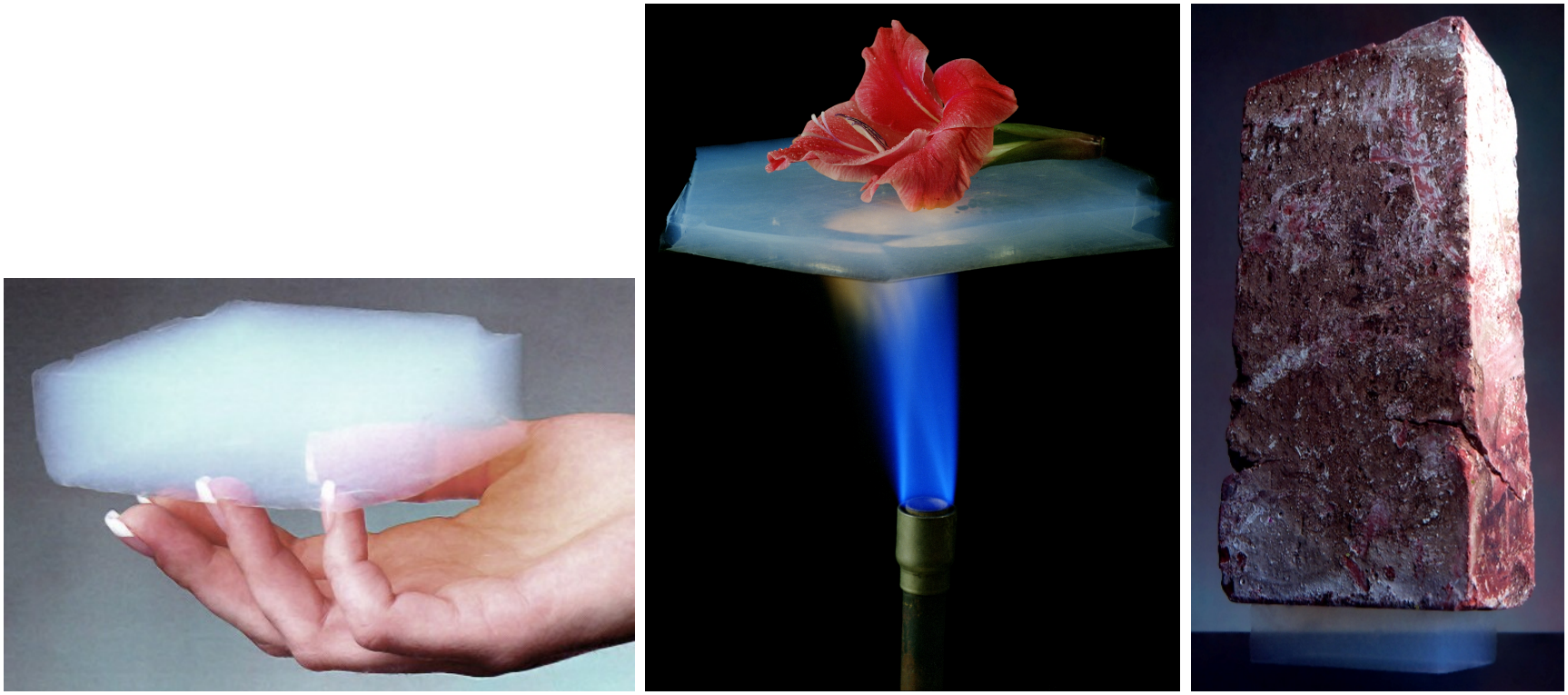
Steel type 304 [13]



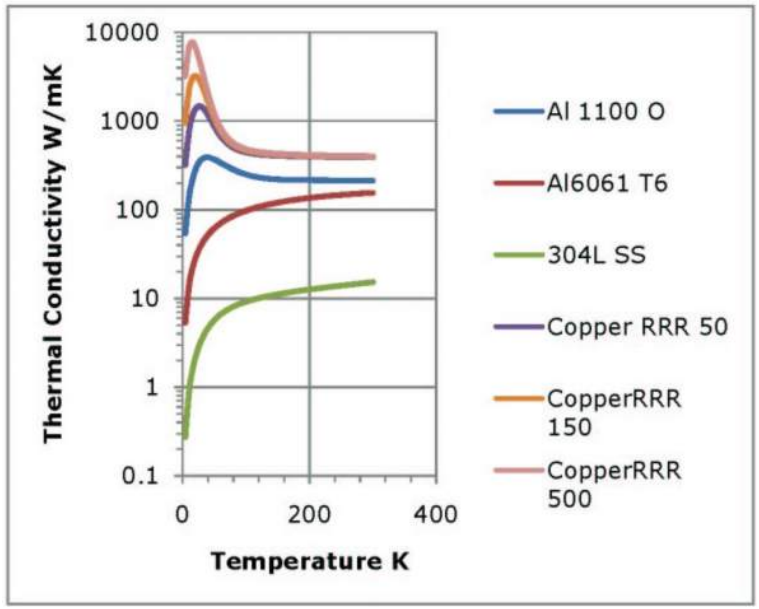
Steel type 316L [13]

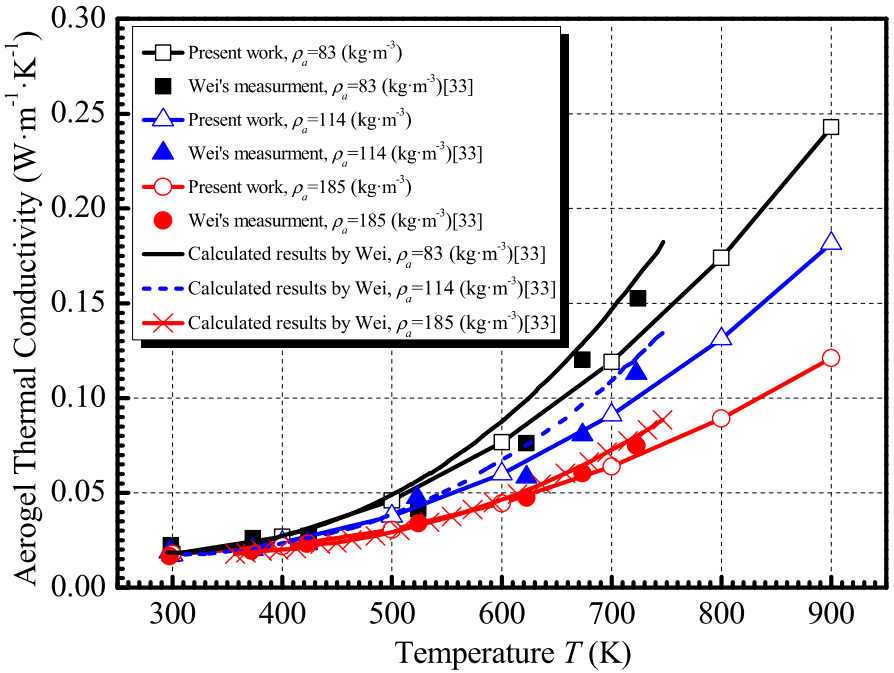


Martensite transformation induced hydrogen cracking at -60 °C [13].
Steel type 304 = austeno-ferritic
Steel type 316L = austenitic



Aerogel [14]. *Left:* A block of silica aerogel. *Middle:* A flower resting on a piece of silica aerogel, which is suspended over a flame from a Bunsen burner. *Right:* A 2.5 kg brick supported by a piece of aerogel with a mass of 2 g.

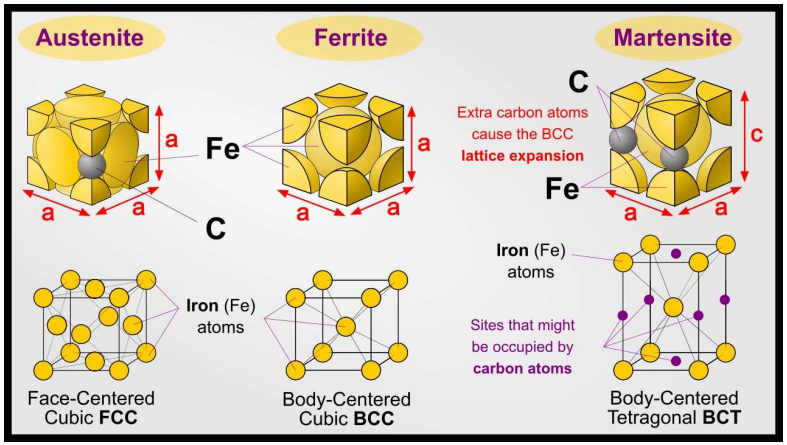


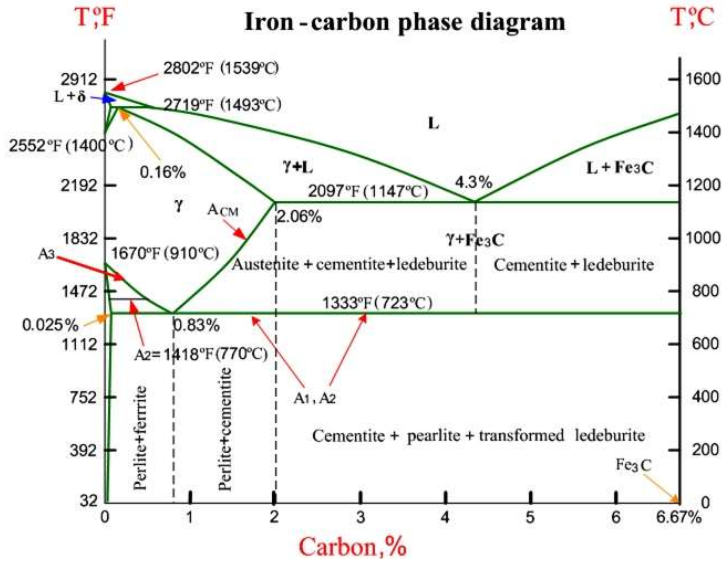


Thermal Conductivity
Left: Steel, aluminium & copper. Data from NIST [15]. *Right:* Aerogel [16].

Note
Thermal conductivity and electrical resistance are inversely related in metals due to free electrons. Their ratio is proportional to temperature in accordance with the Wiedemann-Franz law [17]. Therefore, good electrical conductors (low resistance) are good thermal conductors (high conductivity), and vice versa.
See also: phonon-electron interaction, superconductivity, Cooper pairs.

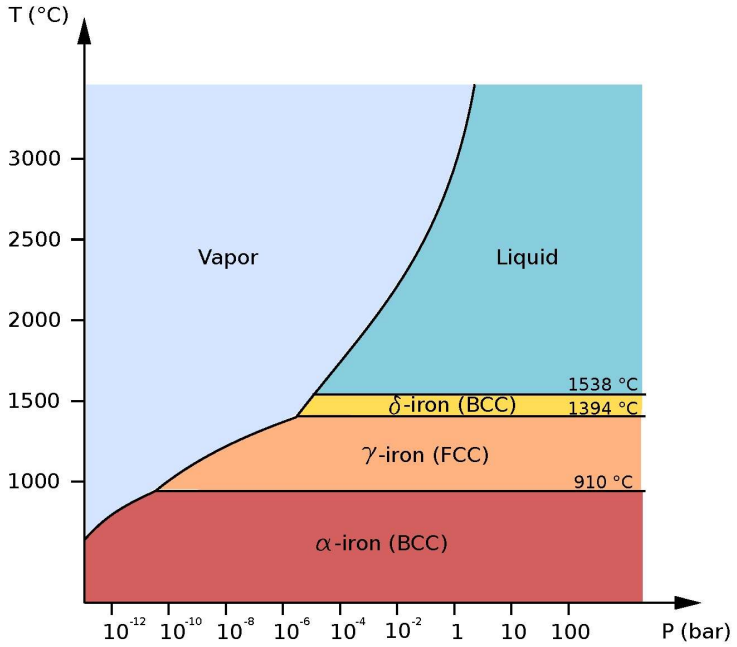
CLASSIFICATION OF STEELS: AUSTENITIC, FERRITIC, MARTENSITIC



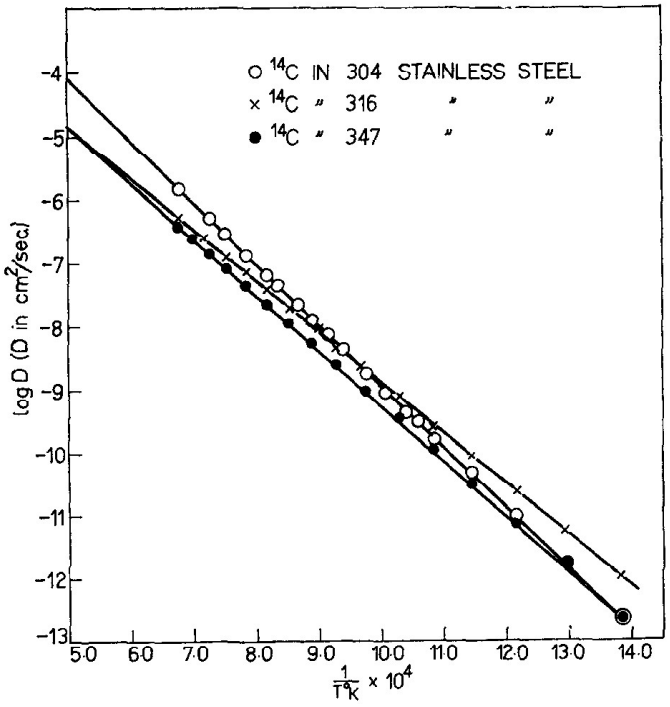


- **At atmospheric pressure, three allotropic forms of iron exist, depending on temperature: alpha iron (α-Fe, ferrite), gamma iron (γ-Fe, austenite), and delta iron (δ-Fe).**
- **Magnetically, α-iron is paramagnetic at high temperatures. However, below its Curie temperature of 771 °C it becomes ferromagnetic.**

Iron phase diagram



DIFFUSION OF CARBON IN STAINLESS STEELS



Concentration gradient [18]:

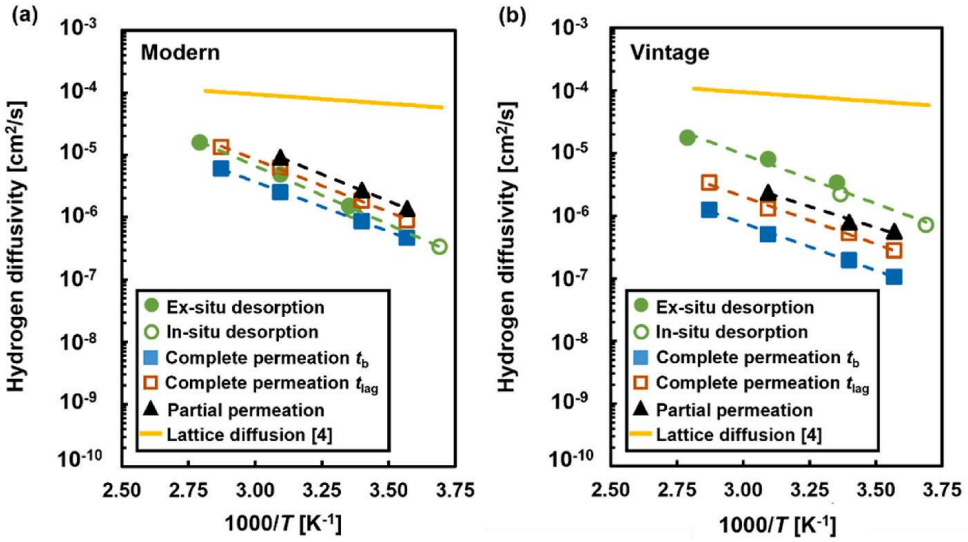
$$-\frac{dc}{dx} = \left[\frac{c}{\sqrt{\pi \mathbb{D} t}}\right] \exp\left[-\frac{x^2}{4\mathbb{D}t}\right]$$

$$\text{where} \quad \mathbb{D} = A \exp\left[-\frac{B}{RT}\right]$$

Type of steels	Time (sec)	Temperature (°C)	Diffusion coefficients (cm^2/sec)
316	1.44×10^5	450	9.31×10^{-13}
	1.44×10^5	500	5.11×10^{-12}
	2.88×10^4	550	1.78×10^{-11}
	7.2×10^3	600	8.28×10^{-11}
	7.2×10^3	650	2.57×10^{-10}
	3.6×10^3	700	7.59×10^{-10}
	7.2×10^3	710	9.55×10^{-10}
	7.2×10^3	760	2.29×10^{-9}
	1.8×10^3	800	4.57×10^{-9}
	1.8×10^3	850	8.71×10^{-9}
	1.8×10^3	900	1.95×10^{-8}
	1.8×10^3	950	3.80×10^{-8}
	1.8×10^3	1000	7.94×10^{-8}
	3.6×10^3	1050	1.20×10^{-7}
	1.8×10^3	1120	2.51×10^{-7}
	1.8×10^3	1200	5.25×10^{-7}

Composition of two X65 steels and the diffusion coefficient of hydrogen [19].

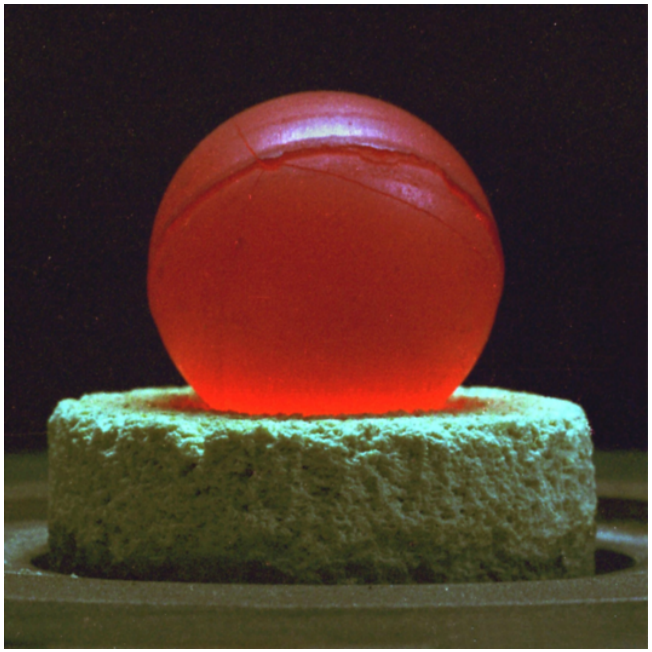
Modern	Element	C	Si	Mn	P	S	Cu	Cr
	wt%	0.07	0.22	1.19	0.011	0.003	0.14	0.15
	Element	Ni	Mo	V	Nb	Ti	N	Fe
	wt%	0.15	0.12	0.02	0.019	0.001	0.01	Bal.
Vintage	Element	C	Si	Mn	P	S	Cu	Cr
	wt. %	0.1	<0.6	<1.6	<0.025	<0.015	<0.25	<0.25
	Element	Ni	Mo	V	Nb	Ti	N	Fe
	wt. %	<0.25	<0.05	<0.1	<0.05	<0.02	<0.01	Bal.



Steel	Temperature [°C]	$D_{eff}(t_b)$ [cm^2/s]
Modern	7	4.62×10^{-7}
	21	8.56×10^{-7}
	50	2.57×10^{-6}
	75	6.04×10^{-6}
Vintage	7	1.05×10^{-7}
	21	1.95×10^{-7}
	50	5.05×10^{-7}
	75	1.25×10^{-6}

STEEL RADIATION EMISSION - TEMPERATURES AND COLORS

Degrees ℃	Degrees ℉	Color of Metal
200	390	Feint Straw
210	410	Very Faint Straw
220	430	Light Yellow
230	445	Pale Straw Yellow
240	465	Golden Yellow/Dark Straw
250	480	Dark Yellow Brown
260	500	Brown Yellow/Purple
270	520	Brown Purple
285	545	Dark Purple
290	555	Full Blue
300	570	Dark Blue
315	600	Very Dark Blue
330	625	Greyish Blue
427	800	Dark Grey
537	1000	Black Red/Red-grey
600	1110	Brown Red
650	1200	Blood Red
715	1320	Dark Cherry Red
770	1420	Medium Cherry Red
815	1500	Full Cherry Red
843	1550	Bright Orange Red
875	1610	Light Red
930	1705	Orange
990	1815	Orange Yellow
1050	1920	Dark Yellow
1093	2000	Bright Yellow
1100	2010	Light Yellow
1200	2190	White
1400	2550	Beginning to sparkle
1500	2730	Melting



Plutonium $\left({}^{238}_{94}\mathrm{Pu}\right)$
Emissive Radiation

CLASSIFICATION OF STEELS: AUSTENITIC, FERRITIC, MARTENSITIC

Steel type	Strength range (MN/m^2)	Characteristic properties
Austenitic	200–500	Non-hardenable except by cold working. Very high toughness. Very good formability. Creep resistant. Non-magnetic. Very good corrosion resistance. High cost.
Ferritic	250–500	Good formability. Inferior corrosion resistance to austenitic steels. High temperature oxidation resistance. Lower cost than austenitic steels.
Martensitic	400–2000	High strength and wear resistance. Inferior toughness.
Precipitation hardened	500–1640	High strength. High toughness. Optimum creep properties. High cost.

Source: Ref [1]. Strength range refers to *Yield Strength.*

COMPOSITION AND PROPERTIES OF AUSTENITIC STEEL

Nominal composition (%)					AISI Type	Effect on properties
Cr	Ni	Mo	C max	Other elements		
18	8	–	0.15		302	Basic steel
17	7	–	0.15		301	Lower Cr and Ni for greater work hardening
18	8	–	0.15	S or Se 0.15 min	303	S added for enhanced machinability
19	10	–	0.08		304	Lower C for improved ductility and weldability
19	10	–	0.03		304L	Lower C for welding of thicker sections
18	11.5	–	0.12		305	Higher Ni for increased formability
23	13.5	–	0.20		309	Higher Cr and Ni for corrosion and scaling resistance
25	20.5	–	0.25		310	Highest Cr and Ni to increase scaling resistance
24.5	20.5	–	0.25	Si 2.75	314	Si higher to increase scaling resistance
17	12	–	0.08		316	Mo added for more corrosion resistance
18	10.5	–	0.08	Ti = 5 × C min	321	Ti added to avoid intergranular corrosion
18	11	–	0.08	Nb + Ta = 10 ×C min	347	Nb, Ta added to avoid intergranular corrosion
18	3.5–6.0	–	0.15	Mn 5.5×10.0 N 0.25 max		Substitution of nickel by manganese gives similar corrosion resistance at lower cost. Strength is approximately 50% higher but weldability is impaired

Type 304 steel is austeno-ferritic. It contains 8 to 20% ferritic steel.
Source: Ref [1].

COMPOSITION AND PROPERTIES OF FERRITIC STEEL

Composition (wt%)						Mechanical properties					Remarks
C	Mn	Si	Cr	Mo	Nb (or Ta)	Condition	0.2% Proof strength (Mn/m^2)	Tensile strength (Mn/m^2)	Reduction of area (%)	Impact toughness (Joules)	
0.08 max	1.0 max	1.0 max	12.0 14.0	–	–	Annealed cold worked	240 520	450 600	60	50	Good formability
0.12 max	1.0 max	1.0 max	14.0 18.0	–	–	Annealed cold worked	300 550	520 650	60	–	Free machining grades containing 0.15% sulfur available
0.12 max	1.0 max	1.0 max	16.0 18.0	0.75 1.25	5 × C	Annealed	350	550	60	–	Improved corrosion resistance and weldability
0.20	1.5	1.0 max	23.0 27.0	–	–	Annealed	375	575	45	5	Excellent resistance to high temperature corrosion and scaling

Source: Ref [1]. Strength range refers to *Yield Strength.*

COMPOSITION AND PROPERTIES OF MARTENSITIC STEEL

Composition (wt%)						Typical mechanical properties			Remarks
C	Mn	Si	Cr	Ni	Mo	0.2% Proof strength (Mn/m^2)	Tensile strength (Mn/m^2)	Impact toughness (Joules)	
0.15 max	1.0 max	1.0 max	11.5–13.5	–	–	400–1020	630–1350	50–100	For high strength tempering temperatures of 150–180°C are employed. For optimum toughness tempering temperatures of 650–750°C are recommended.
0.15 max	1.0 max	1.0 max	11.5–13.5	1.25–2.50	–	720–1050	850–1400	60	
0.15–0.20	1.0 max	1.0 max	12.0–14.0	–	–	1350	1600	15	High strength and wear resistance.
0.20 max	1.0 max	1.0 max	15.0–17.0	1.25–2.50	–	650–1100	875–1400	50	High strength with toughness
0.60–0.75	1.0 max	1.0 max	16.0–18.0	–	0.75 max	1150	1825	6	
0.75–0.95	1.0 max	1.0 max	16.0–18.0	–	0.75 max	1900	1950	4	Very high strength and wear resistance. Very low toughness.
0.95–1.20	1.0 max	1.0 max	16.0–18.0	–	0.75 max	1920	1980	3	

Source: Ref [1]. Strength range refers to *Yield Strength.*

France & Netherlands



IMPLICATIONS FOR THE DUTCH NATURAL GAS TRANSMISSION NETWORK

- **The Dutch Natural Gas Transmission Network is incompatible with hydrogen. And it cannot be repurposed for hydrogen service!**
- Because it is constructed from steel types (X42,..., X70, etc). These are inadequate for hydrogen service. As evidenced by Refs. [6–9, 11, 20]. It are ferritic steels with a composition as summarized on Slide 16.
- **Moreover:** the hydrogen content may not exceed 0.2 vol% within the current/existing natural gas transmission network
- AISI 316L appears to be the only viable option. And that's precisely what is applied for the hydrogen gas transmission network on Slide 34
- Hydrogen embrittlement/damage is caused by a multitude of mechanisms. As per Slide 2. Construction materials for hydrogen service must cope with all these mechanisms simultaneously.
- The NIPV [21], KIWA [22], DNVGL [23] and CE Delft [24] reports are scientifically wrong and misleading. And must be deemed invalid
- Hyperlink to Artificial Intelligence Evaluation

SUPPLEMENTARY LECTURES

- Blast Scaling:
  Explosion Effects on Equipment, Structures, People and the Environment
- Hydrogen Storage: A Concise Overview
- Explosions:
  Phenomenology, Dynamics and Mitigation

HYNETWORK [25]
DUTCH HYDROGEN BACKBONE

New Pipelines:	L360NE (X52) [26] L415NE (X60) [27]
Existing Pipelines:	API5L L245 (Grade B) [28] API5L L360 (X52) [26]
Residual Lifetime:	Calculation Methods [29, 30]

SUPPLEMENTARY REFERENCES

- Refs. [31–45]

Bibliography

[1] Ahmad Z. *Principles of Corrosion Engineering and Corrosion Control*. Butterworth-Heinemann/IChemE Series. Elsevier, Amsterdam, 2006.

[2] Djukic M.B. Hydrogen Embrittlement and Material Selection. Webinar, September 2022.

[3] McGuire M., Zamanzadeh M., Zolfaghari F., and Chikkam A.K. Hydrogen Measurement and Failure Prediction. Matergenics Inc, Pittsburgh, Pennsylvania, USA, August 2025.

[4] Boot T., Kömmelt P., Brouwer H.J.C., Böttger A., and Popovich V. Effect of titanium and vanadium nanocarbide size on hydrogen embrittlement of ferritic steels. *Materials Degradation*, 9: Article 2, 2025.

[5] Djukic M.B., Bakic G.M., Zeravcic V.S., Sedmak A., and Rajicic B. The synergistic action and interplay of hydrogen embrittlement mechanisms in steels and iron: Localized plasticity and decohesion. *Engineering Fracture Mechanics*, 216: Article 106528, 2019.

[6] Koyama M., Akiyama E., , Lee Y.-K., Raabe D., and Tsuzaki K. Overview of hydrogen embrittlement in high-Mn steels. *International Journal of Hydrogen Energy*, 42:12706–12723, 2017.

[7] Martin M.L., Connolly M.J., DelRio F.W., and Slifka A.J. Hydrogen embrittlement in ferritic steels. *Applied Physics Reviews*, 7: Article 041301, 2020.

[8] Moro I., Briottet L., Lemoine P., Andrieu E., Blanc C., and Odemer G. Hydrogen embrittlement susceptibility of a high strength steel X80. *Materials Science and Engineering A*, 527:7252–7260, 2010.

[9] Zhao Z., Qiao G., Tang L., Zhu H., Liao B., and Xiao F. Fatigue properties of X80 pipeline steels with ferrite/bainite dual-phase microstructure. *Materials Science and Engineering A*, 657:96–103, 2016.

[10] Örnek C., Reccagni P., Kivisakk U., Bettini E., Engelberg D.L., and Pan J. Hydrogen embrittlement of super duplex stainless steel – Towards understanding the effects of microstructure and strain. *International Journal of Hydrogen Energy*, 43:12543–12555, 2018.

[11] Raabe D., Sun B., Kwiatkowski Da Silva A., Gault B., Yen H.-W., Sedighiani K., Thoudden Sukumar P., Souza Filho I.R., Katnagallu S., Jägle E., Kürnsteiner P., Kusampudi N., Stephenson L., Herbig M., Liebscher C.H., Springer H., Zaefferer S., Shah V., Wong S.-L., Baron C., Diehl M., Roters F., and Ponge D. Current challenges and opportunities in microstructure-related properties of advanced high-strength steels. *Metallurgical and Materials Transactions A*, 51:5517–5586, 2020.

[12] Zhou X., Tehranchi A., and Curtin W.A. Mechanism and prediction of hydrogen embrittlement in fcc stainless steels and high entropy alloys. *Physical Review Letters*, 127: Article 175501, 2021.

[13] Motomichi K., Wen Y., Hojo T., Ajito S., Kawamori M., and Akiyama E. Factors controlling transformation-induced hydrogen desorption and hydrogen-reduced transformability in austenitic steels clarified via dynamic hydrogen detection during cryogenic deformation. *Scripta Materialia*, 265: Article 116749, 2025.

[14] Wikipedia Encyclopedia. Aerogel. Url: `https://en.wikipedia.org/wiki/Aerogel`.

[15] National Institute of Standards and Technology (NIST). Url: `https://en.wikipedia.org/wiki/National_Institute_of_Standards_and_Technology`.

[16] He Y.-L. and Xie T. Advances of thermal conductivity models of nanoscale silica aerogel insulation material. *Applied Thermal Engineering*, 81:28–50, 2015.

[17] Wikipedia Encyclopedia. Wiedemann-Franz Law. Url: `https://en.wikipedia.org/wiki/Wiedemann-Franz_law`.

[18] Agarwala R.P., Naik M.C., Anand M.S., and Paul A.R. Diffusion of carbon in stainless steels. *Journal of Nuclear Materials*, 36:41–47, 1970.

[19] Koren E., Yamabe J., Lu X., Hagen C.M.H., Wang D., and Johnsen R. Hydrogen diffusivity in X65 pipeline steel: Desorption and permeation studies. *International Journal of Hydrogen Energy*, 61:1157–1169, 2024.

[20] Hoschke J., Fahdul Wahab Chowdhury Md., Roethig M., Tapia-Bastidas C.V., Venezuela J., Shu Y., Gray E., Djukic M.B., Depover T., Verbeken K., and Atrens A. The influence of subcritical annealing and cold working on the hydrogen embrittlement susceptibility of X65 D pipeline steel. *Safety Science*, 2025:1–19, 2025.

[21] Spoelstra M.B. and Reinders J. Reactie NIPV op artikel over veilig gebruik van waterstof in bestaande aardgasleidingen. Nederlands Instituut Publieke Veiligheid (NIPV), November 2024.

[22] Hermkens R., Jansma S., Van der Laan M., De Laat H., Pilzer B., and Pulles K. Toekomstbestendige gasdistributienetten. KIWA Report GT-170272, July 2018.

[23] Van den Noort A., Sloterdijk W., and Vos M. Verkenning waterstofinfrastructuur. DNV GL Report OGNL.151886, July 2017.

[24] Jongsma C., Van der Veen R., and Vendrik J. Waterstof voor de gebouwde omgeving. CE Delft Report 20.190307.001, February 2020. Kennisdocument voor de gemeente Nijmegen.

[25] HyNetwork. Conceptvoorstel aanpassing uitrolplan. Consultatiedocument, 2024.

[26] Bouledroua O., Zelmati D., Hafsi Z., and Djukic M.B. Hydrogen embrittlement effects on remaining life and fatigue crack growth rate in API 5L X52 steel pipelines under cyclic pressure loading. *Engineering Failure Analysis*, 166: Article 108917, 2024.

[27] Faucon L.E., Boot T., Riemslag T., Scott S.P., Liu P., and Popovich V. Hydrogen-Accelerated Fatigue of API X60 Pipeline Steel and its Weld. *Metals*, 13: Article 563, 2023.

[28] Paiva V.E.L., Vieira R.D., and Freire J.L.F. Fatigue Properties Assessment of API 5L Gr. B Pipeline Steel Using Infrared Thermography. In A. Baldi, S. Quinn, X. Balandraud, and J.M. Dulieu-Barton, editors,

Residual Stress, Thermomechanics & Infrared Imaging, Hybrid Techniques and Inverse Problems, volume 7 of *Conference Proceedings of the Society for Experimental Mechanics Series*, pages 17–23, New York, 2019. The Society for Experimental Mechanics, Inc., River Publishers.

[29] Oesterlin H., Fischer C., and Michler T. Evaluation of lifetime predictions for future hydrogen pipelines by different fracture mechanics-based design codes. *Energy Technology*, 13: Article 2301012, 2025.

[30] Yang R., Schell C.A., Rayasam D., and Groth K.M. Hydrogen impact on transmission pipeline risk: Probabilistic analysis of failure causes. *Reliability Engineering and System Safety*, 257A: Article 110825, 2025.

[31] Shtoyko I., Toribio J., Kharin V., and Hredil M. Prediction of the residual lifetime of gas pipelines considering the effect of soil corrosion and material degradation. *Procedia Structural Integrity*, 16:148–152, 2019.

[32] Gallon N. Hydrogen Pipelines – Design and Material Challenges and Mitigation. EPRG Project 221/2020, European Pipeline Research Group (EPRG), December 2020.

[33] Martin P., Ocko I.B., Esquivel-Elizondo S., Kupers R., Cebon D., Baxter T., and Hamburg S.P. A review of challenges with using the natural gas system for hydrogen. *Energy Science and Engineering*, 12:3995–4009, 2024.

[34] Turcott S. *Decoding Mechanical Failures: The Definitive Guide to Interpreting Fractures*. Steel Empire Incorporated, 2020.

[35] American Petroleum Institute (API). Damage Mechanisms Affecting Fixed Equipment in the Refining Industry. API Recommended Practice 571 (API RP 571), 2020.

[36] American Petroleum Institute (API). Thread Compounds for Casing, Tubing, Line Pipe, and Drill Stem Elements. API Recommended Practice 5A3 (API RP 5A3), 2023.

[37] American Petroleum Institute (API). Recommended Practice for Care and Use of Casing and Tubing. API Recommended Practice 5C1 (API RP 5C1), 2025.

[38] American Petroleum Institute (API). Recommended Practice for Conducting Drop-Weight Tear Tests on Line Pipe. API Recommended Practice 5L3 (API RP 5L3), 2025.

[39] American Petroleum Institute (API). Materials and Fabrication of 2.25Cr – 1Mo, 2.25Cr – 1Mo – 0.25V, 3Cr – 1Mo, and 3Cr – 1Mo – 0.25V Steel Heavy-wall Pressure Vessels for High-temperature, High-pressure Hydrogen Service. API Recommended Practice 934-A (API RP 934-A), 2025.

[40] American Society for Testing and Materials (ASTM). Process Piping: ASME Code for Pressure Piping, B31. ASTM International, 2024. Revision of ASME B31.3-2022.

[41] Tao P., Zhou W., Miao X., Peng P., Liu P., and Liu W. Review of characterization on hydrogen embrittlement by micro-sample testing methods. *Metals*, 13: Article 1753, 2023.

[42] Luo H., Sohn S.S., Lu W., Li L., Li X., Soundararajan C.K., Krieger W., Li Z., and Raabe D. A strong and ductile medium-entropy alloy resists hydrogen embrittlement and corrosion. *Nature Communications*, 11: Article 3081, 2020.

[43] Weihrauch M., Patel M., and Patterson E.A. Measurements and predictions of diffusible hydrogen escape and absorption in catholically charged 316LN austenitic stainless steel. *Scientific Repports*, 13: Article 10545, 2023.

[44] Mabho N., Bergers K., Flock J., and Telgheder U. Determination of diffusible and total hydrogen concentration in coated and uncoated steel using melt and solid extraction techniques: Part I. *Talanta*, 82:1298–1305, 2010.

[45] Bergers K., Camisaõ de Souza E., Thomas I., Mabho N., and Flock J. Determination of hydrogen in steel by thermal desorption mass spectrometry. *Steel Research International*, 81:499–507, 2010.